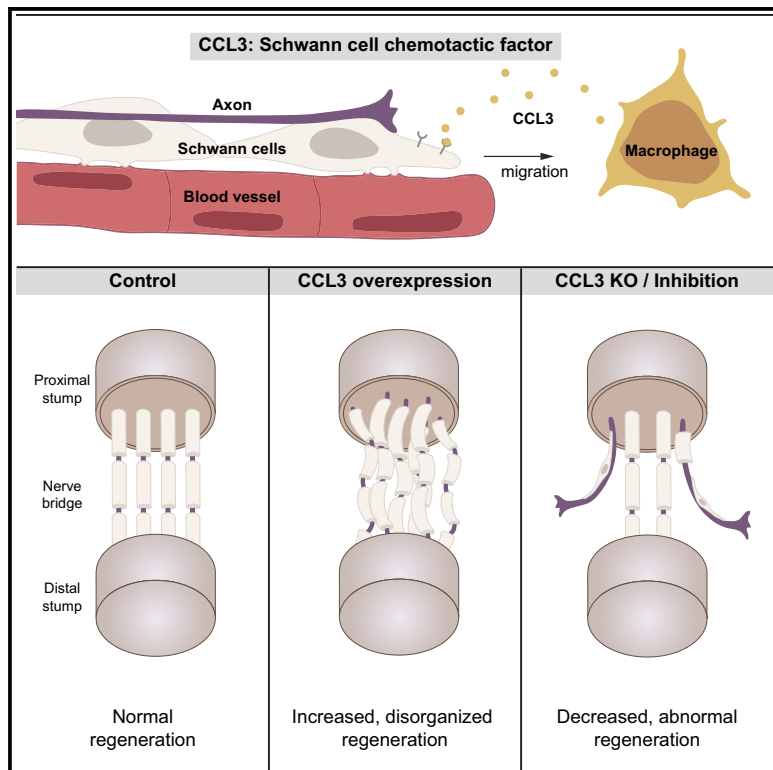


Identification of CCL3 as a Schwann cell chemotactic factor essential for nerve regeneration

Graphical abstract



Authors

Lucie Van Emmenis,
Guillem Mòdol-Caballero,
Elizabeth Harford-Wright, ...,
Inês Boal-Carvalho, Clare L. Bennett,
Alison C. Lloyd

Correspondence

alison.lloyd@ucl.ac.uk

In brief

Van Emmenis, Mòdol-Caballero, and colleagues have identified CCL3 as a Schwann cell chemotactic factor secreted by hypoxic macrophages that is essential for guiding axons during peripheral nerve regeneration. This work further highlights the multicellular complexity of nerve regeneration and that different mechanisms control axon guidance during development and following injury.

Highlights

- CCL3 is an SC chemotactic factor secreted by hypoxic macrophages following injury
- Overexpression of CCL3 causes disorganized SC migration and axonal regrowth
- Loss of CCL3 blocks efficient axonal regrowth *in vivo*, resulting in long-term defects
- Different mechanisms guide SC migration during development and following injury



Article

Identification of CCL3 as a Schwann cell chemotactic factor essential for nerve regeneration

Lucie Van Emmenis,^{1,3} Guillem Mòdol-Caballero,^{1,3} Elizabeth Harford-Wright,¹ Alex Power,¹ Anne-Laure Cattin,¹ Ian J. White,¹ Giulia Casal,¹ Inês Boal-Carvalho,² Clare L. Bennett,² and Alison C. Lloyd^{1,4,*}

¹UCL Laboratory for Molecular Cell Biology, University College London, Gower Street, London WC1E 6BT, UK

²Department of Haematology, UCL Cancer Institute, University College London, London WC1E 6DD, UK

³These authors contributed equally

⁴Lead contact

*Correspondence: alison.lloyd@ucl.ac.uk

<https://doi.org/10.1016/j.celrep.2025.115322>

SUMMARY

Peripheral nerves regenerate following injury, in contrast to those of the central nervous system. This involves the collective migration of Schwann cell (SC) cords, which transport regrowing axons across the wound site. The SC cords migrate along a newly formed vasculature, which bridges the wound site in response to vascular endothelial growth factor, secreted by hypoxic macrophages. However, the directional signals by which SC cords navigate the long distances across the wound, in the absence of those that guide axons during development, remain unknown. Here, we identify CCL3 as the SC chemotactic factor, secreted by hypoxic macrophages, responsible for this process. We show that CCL3 promotes collective SC migration and axonal regrowth *in vivo* and, using genetic mouse models and widely used CCL3 inhibitors, that CCL3 is essential for effective nerve regeneration. These findings have therapeutic implications for both promoting nerve repair and inhibiting the aberrant nerve growth associated with trauma and disease.

INTRODUCTION

Peripheral nerves are able to regenerate following an injury, in contrast to nerves in the central nervous system (CNS), which regenerates poorly.^{1–3} This includes the ability to recover from a transection injury, which requires regrowing axons to cross the wound site, with the resultant formation of new nerve tissue that bridges the gap between the two nerve stumps.^{4,5} However, despite this regenerative potential, a return to full function in patients following a transection injury remains relatively rare, with major injuries frequently requiring a graft, which have limited degrees of success.^{3,6,7} Moreover, imperfect regeneration can also result in the formation of neuromas and neuropathic pain that can be debilitating.^{8–10} There is, therefore, an urgent clinical need to develop new strategies to treat peripheral nerve injuries and to prevent maladaptive regeneration.

Following nerve injury, Schwann cells (SCs), in response to signals from degenerating axons, dedifferentiate to progenitor-like repair SCs that have multiple roles in the regenerative process.^{4,11–13} After the transection of a nerve, the proximal and distal stumps are initially rejoined by the formation of new tissue (the bridge), composed of matrix and inflammatory cells, providing an apparent substantial barrier (~5–10 mm in rats) to axonal regrowth.¹⁴ Previous work has shown that the successful guidance of axonal regrowth across the bridge involves a complex multicellular process that culminates in repair SCs migrating

as cellular cords across the bridge, providing a substrate for and guiding axonal regrowth back into the distal stump.^{4,15}

The collective migration of SCs as cellular cords is an adaptive process triggered by fibroblasts encountered by SCs as they emerge from the nerve stumps into the bridge. SCs typically repulse one another in a process known as contact inhibition of locomotion (CIL), a well-defined mechanism by which migrating cells repel one another, shown to be important for tissue patterning and cell dispersion.¹⁶ As SCs enter an injury site, however, fibroblasts trigger N-cadherin-dependent adhesion between the SCs, leading to the formation of cellular cords,¹⁵ with the persisting CIL repulsive signal providing the outward force that drives their collective migration.¹⁷ However, the SC cords cannot migrate within the matrix of the bridge, requiring a more frictional substrate to gain traction. This is provided by newly formed blood vessels generated in response to a gradient of vascular endothelial growth factor (VEGF) secreted by hypoxic macrophages within the nerve bridge.¹⁴ What remains unknown is how the SC cords successfully find their way across the extensive distances of the bridge in the absence of the guidance signals that direct axonal growth during development.

Collective cell migration is a fundamental mechanism by which cells migrate coordinately and is observed both during development and in pathologies such as cancer and wound repair.^{18–21} Collective cell migration is often driven by the forces of CIL.^{16,22} However, efficient, directed, collective migration also usually



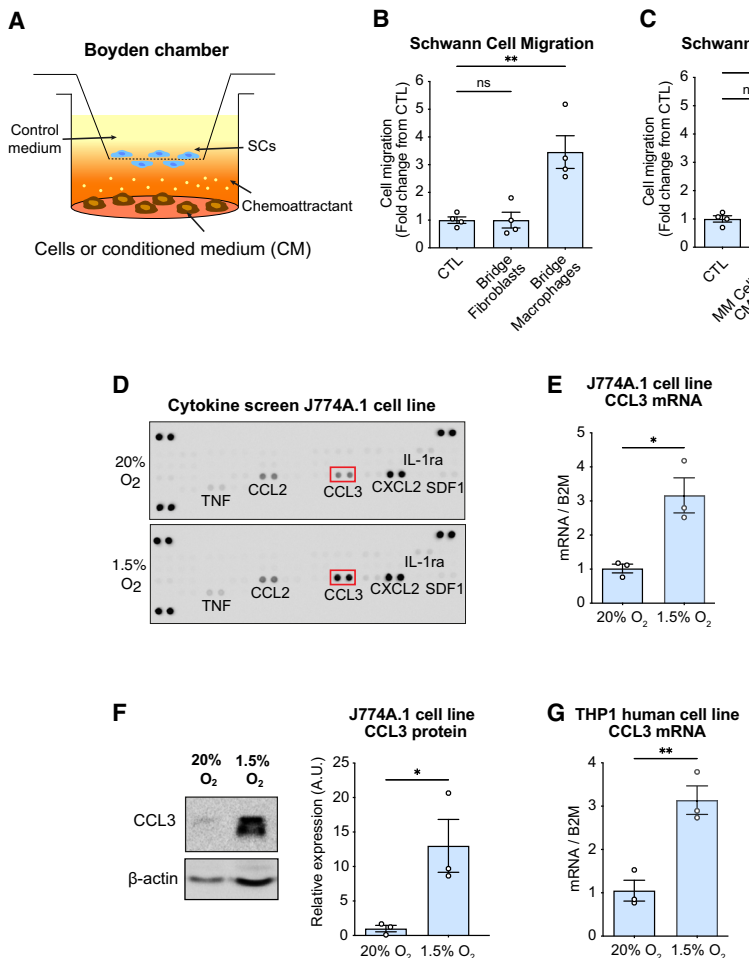


Figure 1. Hypoxic macrophages induce Schwann cell migration

(A) Schematic of the Boyden chamber assay. (B and C) Quantification of Schwann cell (SC) migration in Boyden chamber assays, in response to (B) macrophages or fibroblasts purified from rat nerve bridges ($n = 4$ independent experiments) and (C) conditioned medium (CM) from J774A.1 cells cultured at 20% or 1.5% O_2 ($n = 4$ independent experiments). Control (CTL).

(D) Images of cytokine and chemokine protein array membranes after incubation with CM from J774A.1 cells incubated at 20% or 1.5% O_2 for 48 h.

(E) RT-qPCR analysis of CCL3 mRNA levels in J774A.1 cells cultured in 20% or 1.5% O_2 for 24 h ($n = 3$ independent experiments).

(F) Representative western blot analysis and quantification of CCL3 protein levels in the supernatant of J774A.1 cells incubated at 20% or 1.5% O_2 for 48 h ($n = 3$ independent experiments).

(G) RT-qPCR analysis of CCL3 mRNA expression levels in the human macrophage cell line, THP1 cultured in 20% or 1.5% O_2 for 24 h ($n = 3$ independent experiments).

All data are presented as mean \pm SEM. For (B) and (C), one-way ANOVA test was used. For (E)–(G), an unpaired two-tailed Student's *t* test was used. * $p < 0.05$; ** $p < 0.01$; *** $p < 0.001$; ns, not significant.

See also Figure S1.

requires a chemotactic signal.^{23,24} For example, neural crest cells, the embryonic precursors to SCs, have been shown to migrate collectively in a process driven by CIL, directed by a gradient of the chemoattractant stromal cell-derived factor 1 (SDF1).^{25–27} Following nerve injury, SC cords successfully migrate substantial distances across wound sites; we therefore hypothesized that effective SC migration would also require a chemotactic signal. In this study, we identify the chemokine CCL3 as the SC chemotactic factor secreted by hypoxic macrophages within the wound site. We show that CCL3 expression is essential for the efficient, directed migration of SCs and axons across the wound site, with CCL3 ablation resulting in long-term nerve dysfunction following an injury. Furthermore, we show that increased CCL3 expression leads to aberrant, disorganized structures within a regenerating nerve. These findings have important therapeutic implications for both improving nerve repair and inhibiting aberrant nerve growth associated with pathologies such as neuromas and cancer.

RESULTS

Hypoxic macrophages promote Schwann cell migration

We previously found that hypoxic macrophages isolated from rat nerve bridges were able to stimulate endothelial cell migration

in a VEGF-dependent manner in a Boyden chamber transwell migration assay, mimicking the requirement for macrophage-secreted VEGF to promote the vascularization of the bridge *in vivo*.¹⁴ In

contrast, VEGF did not stimulate SC migration.¹⁴ To test whether stromal cells from the hypoxic nerve bridge were able to stimulate SC migration via a different mechanism, we tested the ability of the two main cell types of the nerve bridge, fibroblasts and macrophages, to stimulate SC migration. To do this, we purified both cell types by immunopanning from Day 2 nerve bridges and placed them in the lower compartment of Boyden chambers (Figures 1A, S1A, and S1B). Analysis of subsequent migration showed that hypoxic bridge macrophages, but not fibroblasts, were able to induce SC migration (Figure 1B). Moreover, we were able to recapitulate these findings using conditioned medium (CM) from a mouse macrophage cell line (J774A.1) cultured in hypoxic conditions (Figures 1C, S1C, and S1D), confirming that hypoxic macrophages also release a factor that increases SC migration.

To identify the factor that was promoting SC migration, we performed an unbiased cytokine screen using CM from the J774A.1 macrophage cell line cultured in low oxygen (1.5% O_2) as compared to "normal" oxygen conditions (20% O_2) and found that CCL3 was strongly upregulated in hypoxic conditions (Figures 1D and S1E). In contrast, the levels of other cytokines, including SDF1 (CXCL12), a chemotactic factor important for neural crest migration, remained unchanged. These results

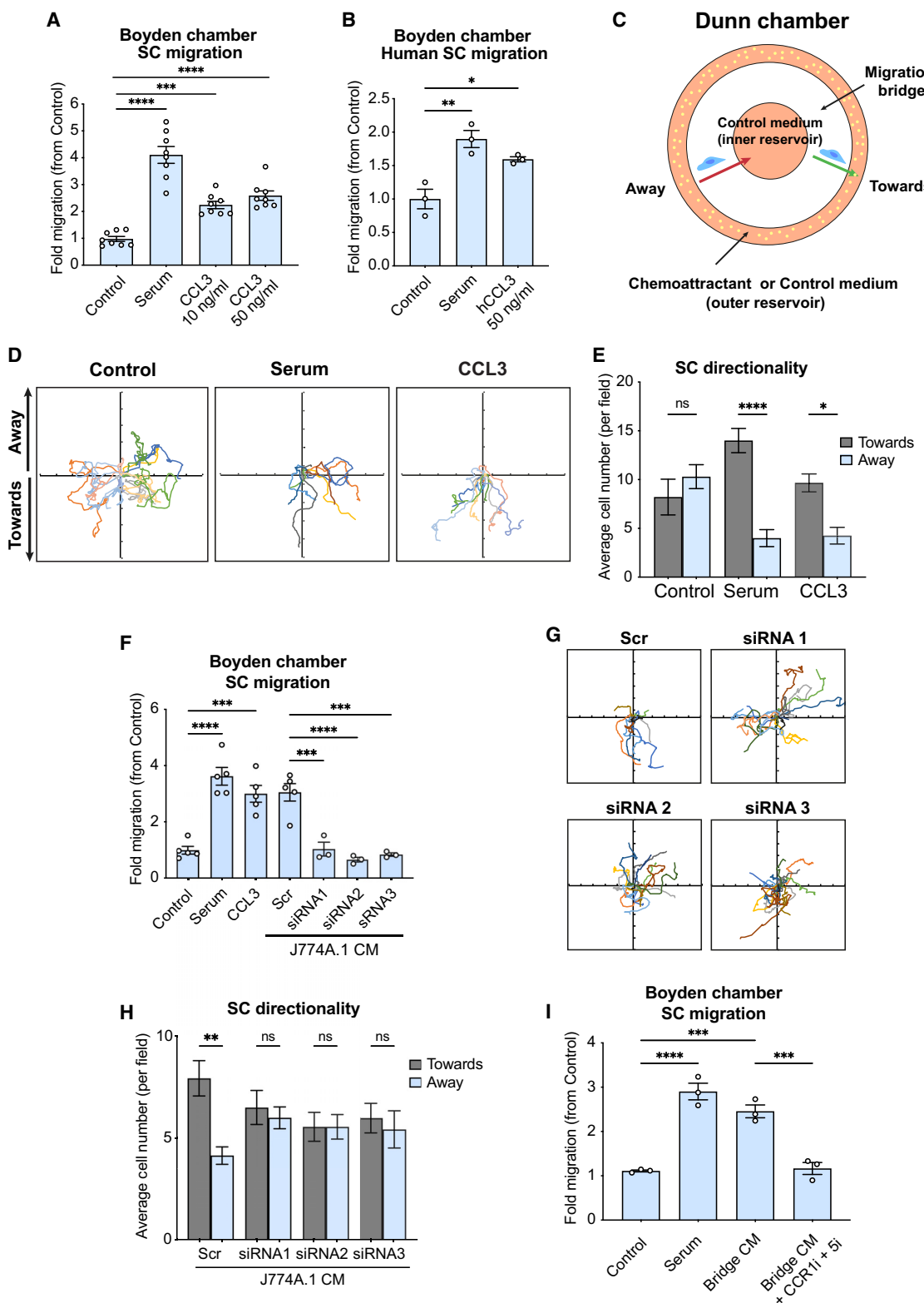


Figure 2. CCL3 is a chemoattractant for Schwann cells

(A) Rat SC migration in Boyden chambers in response to no factors (control), 3% serum (serum), or 10 or 50 ng/ml CCL3 diluted in 0.1% bovine serum albumin/PBS ($n = 8$ independent experiments).

(legend continued on next page)

were validated by both RT-qPCR and western blot analysis (Figures 1E and 1F). A similar response was also observed in a human macrophage cell line (THP1), confirming the conservation of the hypoxic regulation of CCL3 in macrophages (Figure 1G). These findings identified CCL3 as a candidate factor secreted by macrophages that can increase SC migration.

CCL3 is a Schwann cell chemoattractant

To determine whether CCL3 was sufficient to increase SC migration, we initially performed Boyden chamber assays using recombinant CCL3 and found that low concentrations (10 and 50 ng/ml) of CCL3 were sufficient to increase the migration of both rat and human SCs (Figures 2A and 2B). Increased migration in Boyden chamber assays could be due to an increase in the speed and/or in the directionality of the SCs. To test this, we performed Dunn chamber experiments, in which time-lapse analysis allows the quantification of both the speed and directionality of migration (Figures 2C and S2A; Video S1). We found that a gradient of CCL3 significantly influenced the direction of cell migration, but it had no effect on migration speed (Figures 2C–2E, S2A, and S2B), indicating that CCL3 acts as a chemoattractant for SCs. CCL3 signals through the chemokine receptors CCR1 and CCR5, which have been shown to be expressed by rodent repair SCs following their dedifferentiation in response to injury *in vivo*²⁸ (Figure S2C). Moreover, we find that CCR1 upregulation is downstream of the ERK signaling pathway that drives the reprogramming to repair SCs (Figure S2D).¹² To determine whether the CCL3 chemoattractant effect on SCs acted through the known receptors, we used the pharmacological inhibitors J113863 (CCR1 inhibitor) and maraviroc (CCR5 inhibitor) in the Boyden chamber assays.^{29,30} These results showed that CCL3-induced SC migration was reduced to control levels by treatment with either inhibitor (Figure S2E). Moreover, small interfering RNA (siRNA) knockdown of the CCL3 receptor CCR1 produced a similar result (Figures S2F and S2G) that is consistent with CCL3 acting as an SC chemoattractant that requires both CCR1/5 receptors; this is in agreement with reports that the receptors can form heterodimers.³¹

To determine whether CCL3 was the only SC chemoattractant secreted by hypoxic macrophages, we performed an siRNA

knockdown of CCL3 in J774A.1 cells using three independent siRNAs (Figure S2H) and found that CM from siCCL3 knockdown cells was no longer able to stimulate the directional migration of SCs in either Boyden chamber or Dunn chamber assays (Figures 2F–2H). This result was confirmed using CCR1/5 inhibitors in Boyden chamber assays with CM collected from either hypoxic mouse macrophage cells (Figure S2I) or cells isolated from the bridge (Figure 2I). In both cases, migration was reduced to control levels in the presence of the inhibitors. These results identify CCL3 as a conserved SC chemoattractant secreted by hypoxic macrophages and the sole factor responsible for macrophage-induced SC directional migration.

CCL3 is expressed by macrophages within the bridge region

To analyze CCL3 expression within an injured nerve, we performed sciatic nerve transections in rats and harvested the injured nerves at day 2 together with the contralateral uncut nerve. At this time point, the bridge is hypoxic, as blood vessels have yet to vascularize the bridge region.¹⁴ We separated the different regions (proximal, bridge, and distal) and performed RT-qPCR to assess CCL3 expression. We found higher levels of CCL3 mRNA in the nerve bridge compared to the uncut nerve and distal stumps, demonstrating a gradient of expression consistent with CCL3 acting as an SC chemoattractant (Figure 3A). Moreover, these results were confirmed by analysis of macrophages purified from the same regions, with bridge macrophages expressing higher levels of CCL3 compared to those isolated from the proximal or distal stumps (Figure 3B).

To confirm that macrophages preferentially secrete CCL3 within the nerve bridge following injury, we performed *in situ* hybridization chain reaction (HCR)^{32,33} to detect the expression of CCL3 in nerves from control and CCL3 knockout (KO) mice.³⁴ We first crossed these mice to PLP-EGFP mice,³⁵ in which SCs are fluorescently labeled with EGFP, to permit easier detection of SCs within the wound environment. These results showed CCL3 mRNA expression predominantly in macrophages (*Iba1*⁺) within the bridge, whereas the signal was undetectable in CCL3 KO mice (Figures 3C–3E). This result was confirmed using probes to CCR2 mRNA that label the majority of macrophages in

(B) Human SC migration in Boyden chambers in response to control medium, serum, or 50 ng/ml hCCL3 ($n = 3$ independent experiments).

(C) Schematic of a Dunn chamber assay. SCs were seeded onto a coverslip and placed onto the Dunn chamber containing an inner reservoir with control medium containing no factors and an outer reservoir with either control medium, 3% serum culture medium, or control medium containing 50 ng/ml rCCL3. Live imaging of SC migration across the migration bridge between the outer and inner reservoirs was performed for 24 h, and cell migration was tracked to determine the direction of migration either toward or away from the outer chamber.

(D) Representative cell tracks from an individual experiment. The starting point of each cell was normalized to a central starting position and oriented at an angle perpendicular to the gradient.

(E) Quantification of SC migration in response to control medium, serum, or 50 ng/ml CCL3 ($n = 167$ –185 cells quantified per condition, from three independent experiments).

(F) Conditioned medium (CM) collected from J774A.1 cells cultured in hypoxic conditions following treatment with scrambled siRNA (Scr) or CCL3 siRNAs 1–3 and used to assess SC migration in Boyden chambers ($n = 5$ independent experiments for control, serum, CCL3, and Scr; $n = 3$ independent experiments for siRNA1, siRNA2, and siRNA3).

(G) Representative cell tracks from Dunn chamber assays described in (F) and quantified in (H). $n = 100$ –169 cells quantified per condition, from 4 (Scr) and 3 (siRNA CCL3) independent experiments.

(I) SC migration in Boyden chambers in response to no factors (control), serum, or CM from ex vivo bridge cells (bridge CM) cultured in 1.5% O₂ ± CCR1 and CCR5 inhibitors (10 μM CCR1i, J113863; 50 μM CCR5i, maraviroc) ($n = 3$ independent experiments).

Data are presented as mean ± SEM. For (A), (B), (E), (F), (H), and (I), a one-way ANOVA test was used. * $p < 0.05$; ** $p < 0.01$; *** $p < 0.001$; **** $p < 0.0001$; ns, not significant.

See also Figure S2 and Video S1.

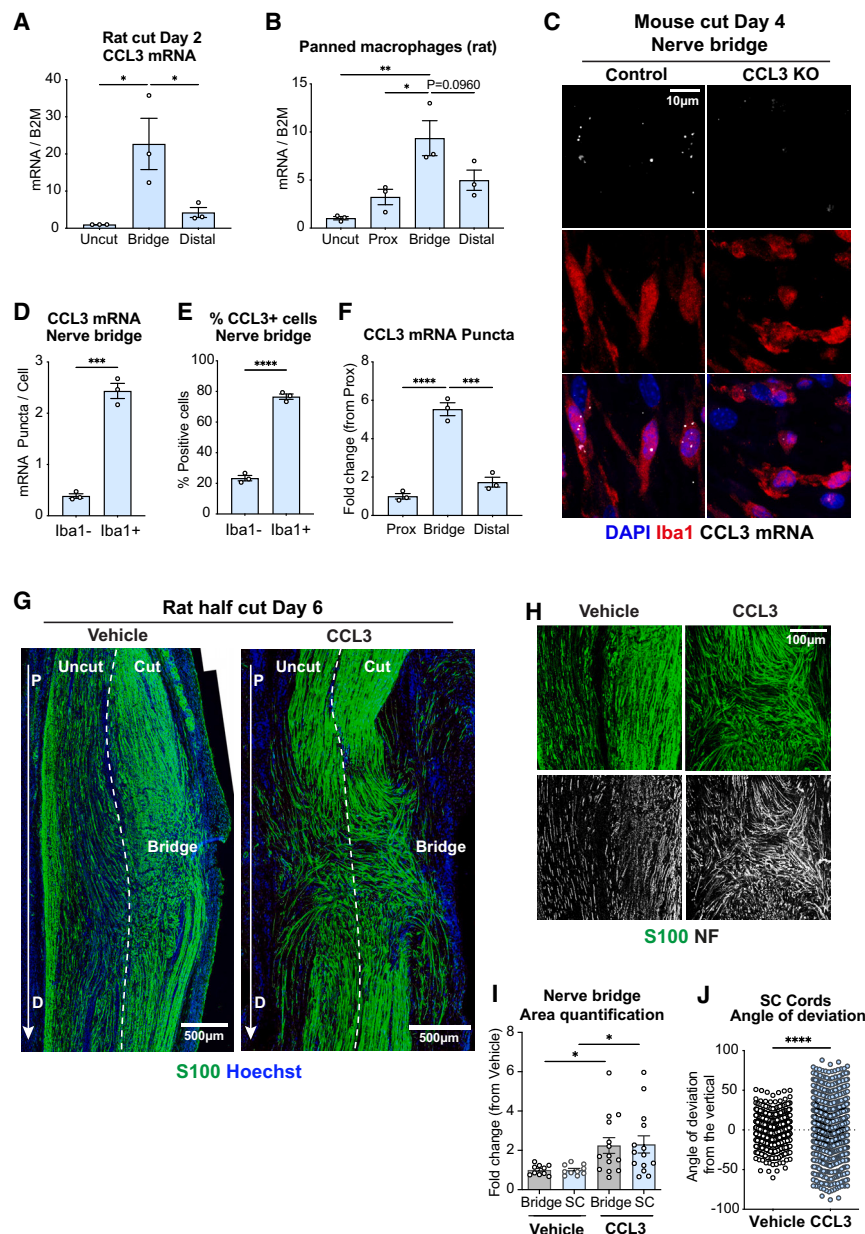


Figure 3. Elevated CCL3 increases Schwann cell migration in a regenerating nerve

(A) RT-qPCR quantification of CCL3 mRNA levels in rat nerve bridge and distal stumps at Day 2 following nerve injury compared to the uncut nerve ($n = 3$ rats).

(B) RT-qPCR quantification of CCL3 mRNA expression in panned CD11b⁺ macrophages purified from uncut nerves (uncut) and injured nerve regions (proximal stump [prox], nerve bridge [bridge], distal stump [distal]) harvested on Day 2 following injury. $n = 3$ independent experiments; three rat nerves were pooled per experiment.

(C) Representative confocal images of Control and CCL3 KO mouse nerve bridges immunostained for Iba1 (red) to detect macrophages together with *in situ* hybridization chain reaction (HCR) to detect CCL3 mRNA (white) at Day 4 post-injury; nuclei are stained with DAPI (blue). Scale bar, 10 μ m.

(D and E) Quantification of (C), showing (D) CCL3 puncta per cell and (E) percentage of CCL3 expressing cells in control Iba1⁺ and Iba1⁻ cells in the nerve bridge ($n = 3$ mice/group).

(F) Quantification of CCL3 puncta in Iba1⁺ cells in the nerve bridge (bridge) and distal stump (distal) relative to the proximal stump (prox) at Day 4 following injury ($n = 3$ mice/group).

(G) Representative confocal images of longitudinal sections of half-cut rat sciatic nerves injected in the nerve bridge with vehicle (5 μ l PBS) or CCL3 (50 μ g/ml) at Day 2 following injury and harvested at Day 6. Sections were immunostained for SCs (S100, green), and nuclei were stained with Hoechst (blue). Dashed lines indicate the intersection between the cut and uncut regions; arrows indicate proximal (P) to distal (D). Scale bar, 500 μ m.

(H) Higher-magnification representative images of the nerve bridges of vehicle and CCL3-injected nerves, showing the organization of SC migration (S100⁺, green) and axonal regrowth (neurofilament [NF], white). Scale bar, 100 μ m.

(I) Quantification of the areas of the nerve bridges and SC area at Day 6 following injury ($n = 10$ vehicle-treated rats, $n = 14$ CCL3-treated rats).

(J) Quantification of the directionality of the SC cords, measured as the angle of deviation from the vertical, in CCL3 and vehicle-treated rats, with 0°–90° deviation to the right counted as positive and to the left counted as negative to demonstrate the spread on both sides of the nerve ($n = 1,120$ SC cords from 10 vehicle-treated rats; $n = 1,485$ SC cords from 14 CCL3-treated rats).

Data are presented as mean \pm SEM. For (A), (B), and (F), one-way ANOVA test was used. For (D), (E), and (I), an unpaired two-tailed Student's t test was used. For (J), an unpaired two-tailed Welch's t test was used. * $p < 0.05$; ** $p < 0.01$; *** $p < 0.001$; **** $p < 0.0001$.

See also Figure S3.

the bridge, which we previously showed are monocyte derived¹⁴ (Figures S3A–S3C). Moreover, comparison to the proximal and distal stumps verified that CCL3 mRNA expression was higher in macrophages within the bridge (Figures 3C–3F and S3D).

Elevated CCL3 induces aberrant Schwann cell migration in a regenerating nerve

To investigate the consequences of increasing the levels of CCL3 within a regenerating nerve, we injected CCL3 or vehicle

(PBS) into the nerve bridge of rat sciatic nerves on Day 2 following surgery, harvesting the nerves at Day 6. For these experiments, we performed half-transections to both reduce experimental variability and to provide an uncut fascicle as a control for each experiment.¹⁵ Strikingly, tile-scan images showed an enlarged bridge region in CCL3-injected nerves containing increased numbers of SC cords and axons (Figures 3G, 3H, and S3E). Quantification of the size of the bridge and area of SC staining indicated that the CCL3-injected nerves were

larger and contained more SC cords (Figure 3I). Despite the effects of CCL3 in producing more SC cords, we did not find that CCL3 significantly increased the proliferation of SCs, as tested in an *in vitro* proliferation assay (Figure S3F). In the CCL3-injected animals, we also observed that the cords of SCs and axons were highly disorganized, including some cords appearing to migrate away from the stumps into surrounding tissue (Figures 3G, 3H, and S3E, and quantified in Figure 3J). In many ways, these structures resemble neuromas, in which aberrant repair results in disorganized tissue consisting of repair SCs and axons.^{36–38} These results show that increased levels of CCL3 within a damaged nerve can increase the migration of SC cords but also result in a disorganized regeneration process.

CCL3 is required for peripheral nerve regeneration following injury

To address the importance of CCL3 for efficient nerve regeneration, we analyzed the repair process using CCL3 KO mice. To determine the effects of CCL3 KO on normal nerve development, we initially characterized the nerves of the mutant mice and found no detectable differences in nerve structure between adult KO and control animals, suggesting that CCL3 does not have a role in the migration of SCs during development (Figures S4A and S4B). As CCL3 has been reported to regulate macrophage behavior,^{39,40} we quantified the number of resident macrophages within adult nerves and also found no significant differences between the CCL3 KO and control nerves (Figures S4C and S4D).

We then tested whether CCL3 was important for nerve regeneration across the wound site following injury. To do this, we performed full sciatic nerve transections and harvested the injured nerves on Day 7, a time point when SCs and axons have normally almost fully migrated across the nerve bridge.^{14,15} We analyzed tile-scan images of longitudinal sections of the nerves and observed a dramatic decrease in SC migration and axonal regrowth across the nerve bridge in mice lacking CCL3 (Figures 4A, 4B and S4E). In control nerves, as expected, we observed that the majority of SC cords traversed the bridge in a directional manner, escorting regrowing axons across the bridge (Figures 4A and 4B). SCs migrate similarly from both stumps, irrespective of the presence of regrowing axons, as we demonstrated previously.¹⁴ In contrast, in CCL3 KO mice, the regenerative process was severely disrupted, with far fewer SC cords successfully crossing the injury site and many SC cords deviating from their normal direction of travel toward surrounding tissue (Figures 4A–4C). Moreover, in some CCL3 KO nerves (two out of eight), the process was grossly disrupted, with all SC cords failing to cross the bridge (Figures 4A and S4E). Consistent with axons requiring SC cords as a substrate to migrate across the bridge, axonal regrowth was similarly affected as they followed the misdirected SC cords (Figures 4D–4F). Importantly, we were able to show that this failure of axonal regrowth did not result from disruption to the initial formation and vascularization of the bridge that occurs prior to SC migration (Figures 4G and 4H), indicating that the role of CCL3 on SC migration is independent of bridge vascularization. Harvesting of nerves at Day 5 showed that the bridges were indistinguishable between the CCL3 KO and control mice, with

nerve bridges of a similar size, shape, and morphology (Figures S4F and S4G). Moreover, we found no differences in macrophage number within the bridges of CCL3 KO and control animals (Figures 4H and 4I). These experiments demonstrate an essential role of CCL3 for SC cords to efficiently migrate across the injury site, with subsequent effects on successful axonal regrowth toward the distal stump.

Pharmacological inhibition of CCL3 receptors disrupts Schwann cell migration into the nerve bridge following injury

Pharmacological inhibition of CCL3 receptors was sufficient to block CCL3-stimulated SC chemotaxis in our *in vitro* assays (Figure S2D). Maraviroc, a CCR5 inhibitor, has been used extensively clinically for the treatment of HIV^{29,41} and is showing promise for the treatment of cancer.⁴² We therefore tested whether pharmacological inhibition of CCR5 could mimic the genetic KO, with implications for therapeutic interventions associated with abnormal nerve growth. In addition, the use of an inhibitor allowed us to inhibit CCL3 after the vascularized bridge had fully formed, ensuring we were solely studying the role of CCL3 on SC migration. To do this, we carried out sciatic nerve transections and treated mice with either vehicle (5% DMSO in water) or 25 mg/kg maraviroc orally twice per day between days 5 and 7 following injury, a time point at which the bridge and vasculature has fully formed,^{14,15} before harvesting on Day 7 (Figure 5A). Remarkably, we observed a very similar phenotype in the maraviroc-treated animals and CCL3 KO mice with severe defects in directional SC migration and axonal regrowth in the treated animals. As expected, the size of the bridges and blood vessel density and polarity was similar between the control and maraviroc-treated animals (Figures 5B, 5C, S5A, and S5B). However, despite the presence of similar structural environments that are conducive to SC cord migration, far fewer SC cords and axons regrew into the bridge in the treated mice (Figure 5B, quantified in Figures 5D and 5E, and Figure S5C), with the SCs exhibiting a similar misdirected phenotype observed in the CCL3 KO mice (Figures 5F and 5G). Collectively, these data show that SCs require the SC chemotactic factor, CCL3, to successfully guide the regrowth of axons across the nerve bridge.

Loss of CCL3 causes long-term defects in nerve regeneration

Our initial analyses showed that CCL3 was required for the normal migration of SC cords across the injury site, consistent with the requirement of a chemotactic factor for effective, directed, and collective migration in other systems.²⁴ To determine whether this resulted in a long-term impairment to repair, we performed longer-term studies. To do this, we performed transection injuries in control and CCL3 KO mice and analyzed the nerves 3 months after injury, a time point when axons normally have regrown and reinnervated their targets, SCs have re-differentiated, and the inflammatory response has largely resolved.^{5,43,44} Tile-scan images of control nerves at 3 months showed a normal regenerated nerve, with the regenerated region of the bridge (which is new nerve tissue) consisting of parallel axons and associated SCs with a similar structure to the distal

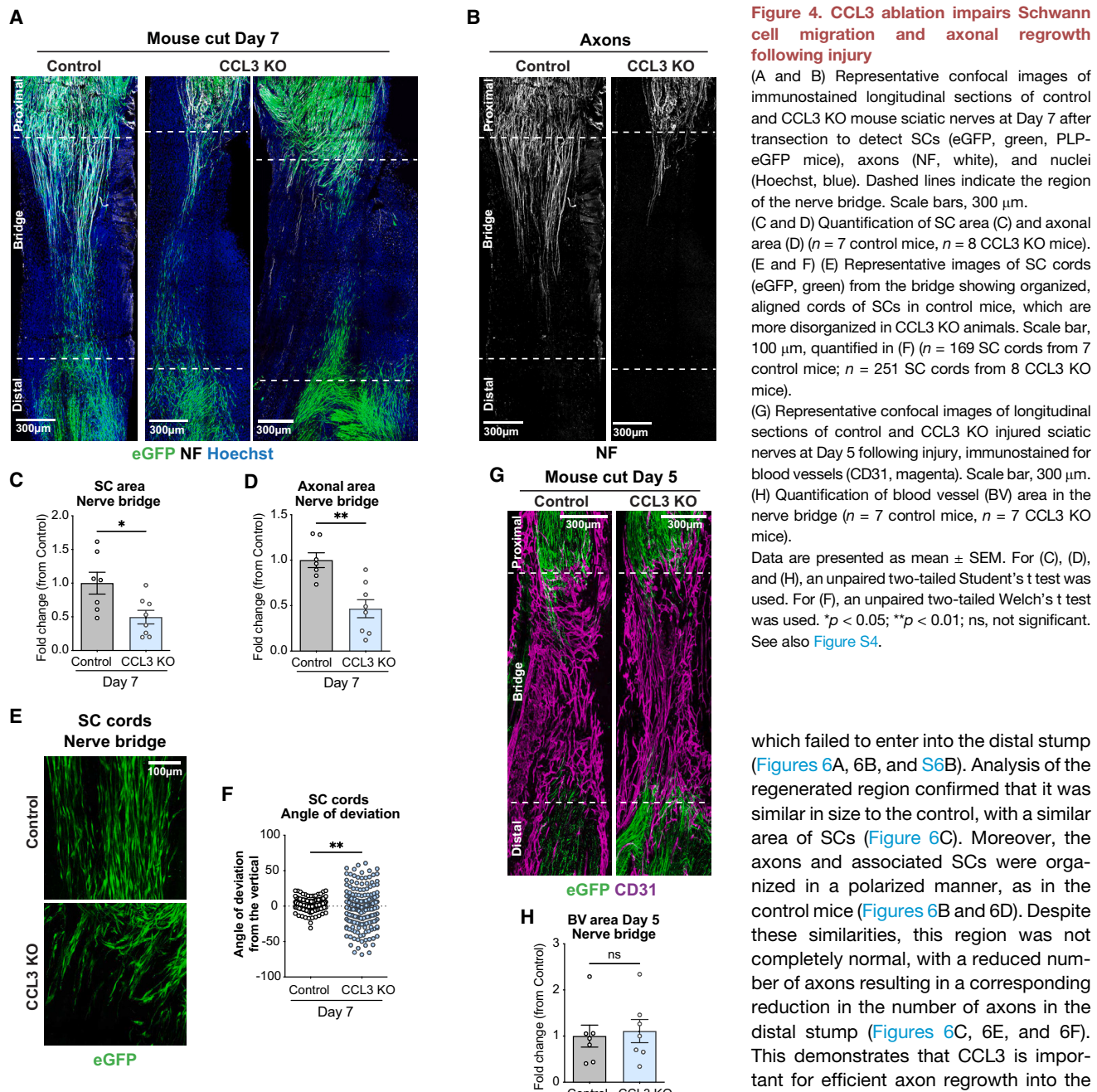


Figure 4. CCL3 ablation impairs Schwann cell migration and axonal regrowth following injury

(A and B) Representative confocal images of immunostained longitudinal sections of control and CCL3 KO mouse sciatic nerves at Day 7 after transection to detect SCs (eGFP, green, PLP-eGFP mice), axons (NF, white), and nuclei (Hoechst, blue). Dashed lines indicate the region of the nerve bridge. Scale bars, 300 μ m.

(C and D) Quantification of SC area (C) and axonal area (D) ($n = 7$ control mice, $n = 8$ CCL3 KO mice). (E and F) (E) Representative images of SC cords (eGFP, green) from the bridge showing organized, aligned cords of SCs in control mice, which are more disorganized in CCL3 KO animals. Scale bar, 100 μ m, quantified in (F) ($n = 169$ SC cords from 7 control mice; $n = 251$ SC cords from 8 CCL3 KO mice).

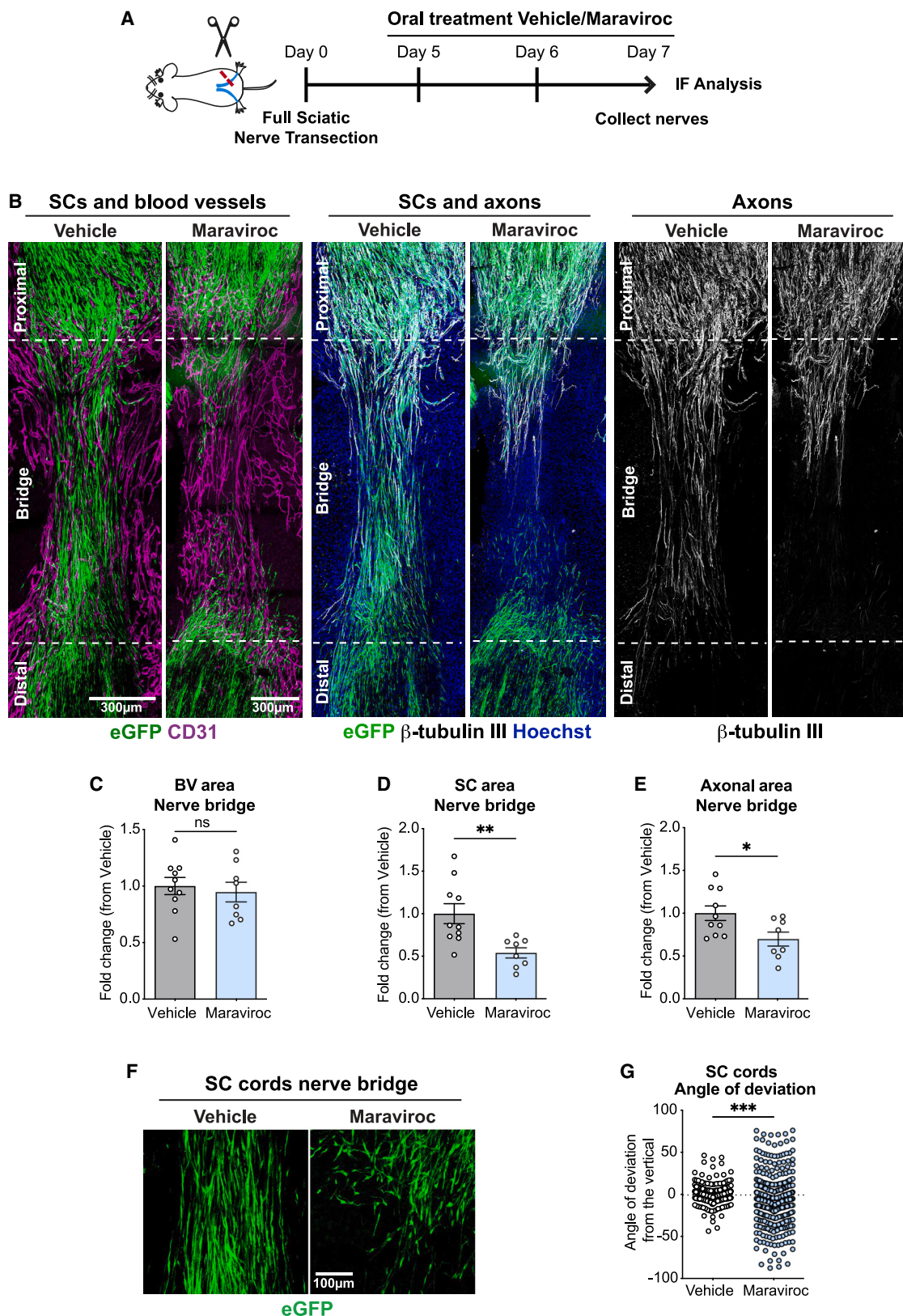
(G) Representative confocal images of longitudinal sections of control and CCL3 KO injured sciatic nerves at Day 5 following injury, immunostained for blood vessels (CD31, magenta). Scale bar, 300 μ m. (H) Quantification of blood vessel (BV) area in the nerve bridge ($n = 7$ control mice, $n = 7$ CCL3 KO mice).

Data are presented as mean \pm SEM. For (C), (D), and (H), an unpaired two-tailed Student's t test was used. For (F), an unpaired two-tailed Welch's t test was used. * $p < 0.05$; ** $p < 0.01$; ns, not significant. See also Figure S4.

stump (Figures 6A and 6B). Consistent with previous studies,⁴⁴ both the regenerated region and the distal stump had an increased number of axons due to increased axonal sprouting during the regenerative process and a corresponding increase in support cells, including SCs (Figure S6A). In contrast, the nerves of CCL3 KO mice were strikingly different, in that they were composed of two distinct regions at the prior site of injury: (1) a regenerated region, which appeared to be similar to the regenerated region in control animals and (2) aberrant regions around the nerve, consisting of SCs and associated axons,

which failed to enter into the distal stump (Figures 6A, 6B, and S6B). Analysis of the regenerated region confirmed that it was similar in size to the control, with a similar area of SCs (Figure 6C). Moreover, the axons and associated SCs were organized in a polarized manner, as in the control mice (Figures 6B and 6D). Despite these similarities, this region was not completely normal, with a reduced number of axons resulting in a corresponding reduction in the number of axons in the distal stump (Figures 6C, 6E, and 6F). This demonstrates that CCL3 is important for efficient axon regrowth into the distal stump, with loss of CCL3 resulting in a decrease in axons returning to reinnervate tissues. More striking, however,

all of the CCL3 KO nerves ($n = 6$ mice) exhibited aberrant regions of axonal regrowth and associated SCs outside of the normal structure (Figures 6A, 6B, 6G, and S6B). Within these regions, the SCs and axons were highly disorganized, lacking the polarization observed in the regenerated regions (Figures 6B–6D and S6C). Interestingly, consistent with an unresolved regeneration process, the majority of the SCs in the aberrant regions remained undifferentiated and were found to be associated with a similarly disorganized vasculature (Figures 7A–7F). In many ways, these persistent disorganized structures resemble neuromas that



form after an aberrant repair process.^{36–38,45} These results show that CCL3, an SC chemotactic factor, is required for effective nerve regeneration, with its absence resulting in both a long-term decrease in axonal regrowth and the formation of abnormal, disorganized axonal/SC structures that resemble neuromas.³⁸

DISCUSSION

For the effective repair of a severed nerve, regrowing axons need to navigate through the apparently hostile environment of the nerve bridge that forms to rejoin the two nerve stumps.^{4,5} This requires a complex multicellular response in which SC cords guide axons across a polarized vasculature.^{14,15} While we have shown previously that the collective migration of the SC cords is driven by the force of CIL,¹⁷ both theoretical models and studies of other cell types have shown that for efficient, directed collective migration, a chemotactic factor is also required.^{46–48} In this study, we identified the chemokine CCL3 as the SC chemoattractant responsible for the effective migration of SC cords across an injury site. As SCs are required to guide regrowing axons across the wound, the absence of CCL3 results in aberrant axonal regrowth leading to long-term failure of the regeneration process. In contrast, we found that overexpression of CCL3 results in an increased number of disorganized SC cords eventuating in aberrant axonal regrowth and structures reminiscent of neuromas. These findings may therefore have important therapeutic implications both for improving nerve repair and inhibiting aberrant repair processes such as neuroma formation.

While CCL3 is important for efficient nerve regeneration, we find that partial regeneration still occurs in the absence of CCL3, indicating it is not the sole factor directing the regenerative response. We have previously shown that the collective migration of SC cords across the injury site is driven by a CIL repulsion signal (N-cadherin/Slit/Robo signaling) that provides an outward force propelling the migrating cords.¹⁷ These forces remain intact in the absence of CCL3 signaling, resulting in SC cords that still migrate out of the stumps but frequently lose their way, leading to the partial abnormalities seen in the longer-term studies.

The collective migration of neural crest cells during development is one of the best-characterized systems of cell migration in animals.²⁶ SCs derive from neural crest cells during embryogenesis, and therefore it might have been expected that similar mechanisms would underlie their migratory behavior. However, it is somewhat surprising that while there are similarities, in that the collective migration of both SCs and neural crest cells are

driven by CIL and in response to a chemotactic factor, the mechanisms and molecules are very different. Neural crests migrate in looser clusters, involving a co-attraction mechanism to maintain cohesion,^{49,50} whereas SCs migrate in cord-like structures, a mechanism that is mediated via ephrin B/Sox2-dependent relocation of N-cadherin to the cell surface.¹⁵ Additionally, several chemokines have been proposed to regulate neural crest cell migration during development, including SDF1.^{24,25} Instead, we have identified macrophage-secreted CCL3 as the chemotactic signal required for the efficient migration of SCs following injury. Interestingly, nerves develop normally in CCL3 KO mice, indicating that the substantial SC migration that occurs during development is controlled by different mechanisms. Indeed, precursor SCs migrate along axons in a neuregulin 1-type III-dependent manner, showing that substrate, directionality, and chemotactic factors all differ between SC developmental and repair processes.^{51,52} However, while the molecules and substrates may differ, our present data reinforce the essential role of chemotactic factors as an essential mechanism for the efficient, directional, collective migration of cells.

We previously showed that hypoxic macrophages within the newly formed nerve bridge initiate axonal regrowth across the wound site by secreting VEGF, which leads to the formation of a polarized vasculature that is subsequently used by the SC cords to cross the injury site.^{4,10,14} Here, we identify an additional role for hypoxic macrophages within the bridge, in that they are also responsible for the secretion of CCL3, demonstrating a dual, coordinated role for macrophages in both inducing the formation of the polarized vasculature on which the SC cords migrate (via VEGF) and directing the subsequent migration of SC cords along them (via CCL3). CCL3 was previously characterized as a macrophage chemotactic factor.^{39,40} However, we found that the loss of CCL3 had no effect either on resident macrophage numbers in normal nerves or the recruitment of macrophages to the wound site after injury. Instead, we show a dramatic effect of the loss of CCL3 on SC migration after injury, in that without the chemotactic factor, the SC cords appeared to migrate less efficiently and frequently became misdirected. This might suggest a therapeutic role for CCL3 in improving the migration of SC cords across grafts that are used to bridge major nerve injuries but often work poorly.⁸ This work also highlights further the myriad roles of macrophages in wound repair and may provide alternative strategies to inhibit aberrant nerve repair in neuromas³⁸ or possibly to target the innervation of tumors.⁵³

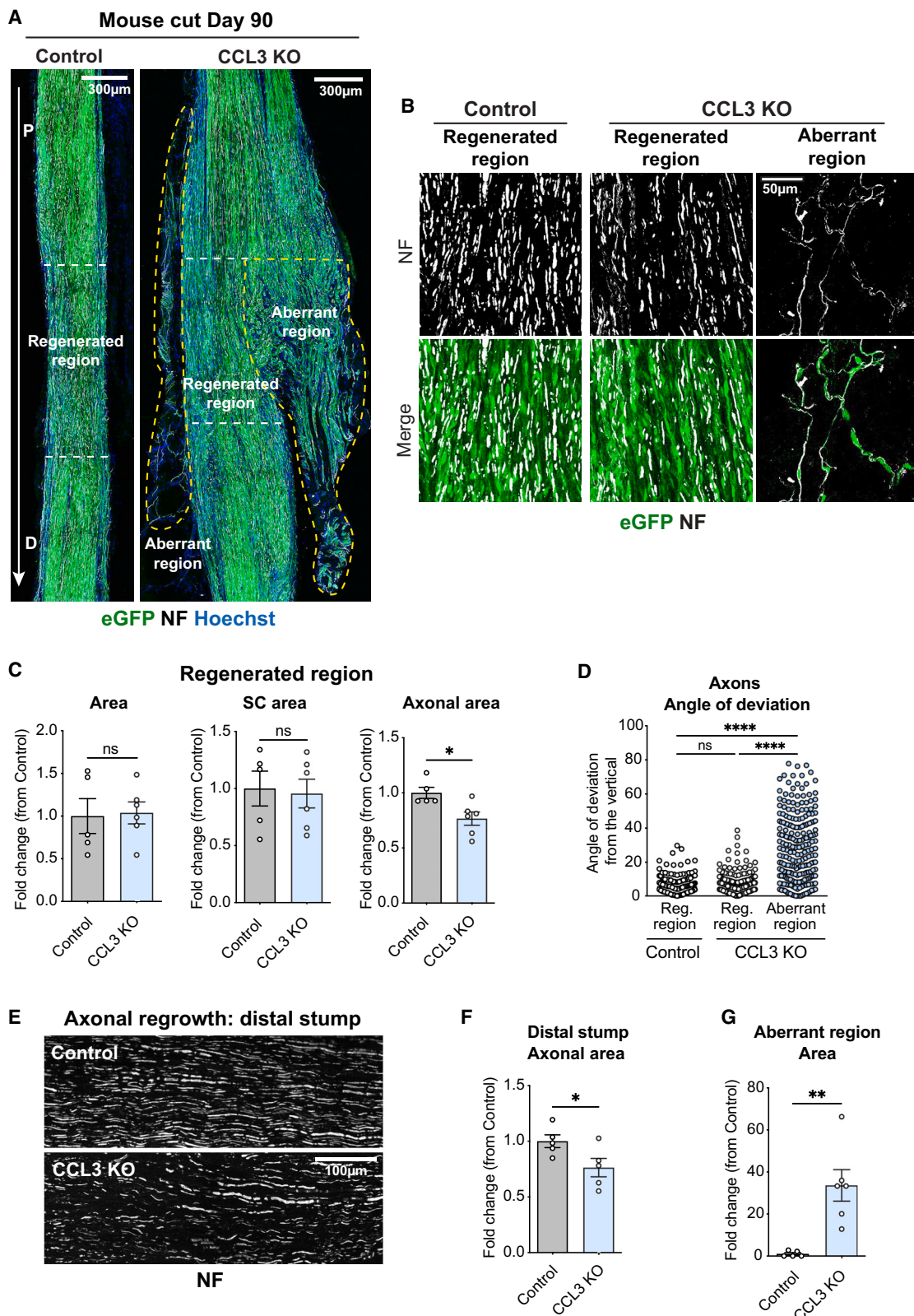
Figure 5. Pharmacological inhibition of CCL3 impairs Schwann cell migration and axonal regrowth following injury

- (A) Schematic showing the experimental design for the inhibitor experiments. PLP-eGFP mice were treated orally with vehicle (5% DMSO in water) or maraviroc (25 mg/kg in 5% DMSO water) twice daily from Days 5–7 after sciatic nerve transection.
- (B) Representative confocal images of longitudinal sections of vehicle- and maraviroc-treated nerves from Day 7, PLP-eGFP mice (SCs, green); immunostained to visualize BVs (CD31, magenta) and axons (β -tubulin III, white) and stained for nuclei (Hoechst, blue). Scale bar, 300 μ m.
- (C–E) Quantification of (C) BV area, (D) SC area, and (E) axonal area ($n = 10$ vehicle mice; $n = 8$ maraviroc-injected mice).
- (F) Higher-magnification representative immunofluorescence images of longitudinal sections of PLP-eGFP mice at Day 7 after injury, treated with vehicle or maraviroc, showing disorganized SC (eGFP, green) migration into the nerve bridge of maraviroc-injected mice. Scale bar, 100 μ m.
- (G) SC cord directionality quantified, as determined by the angle of deviation from the vertical ($n = 360$ SC cords from 10 vehicle-treated mice; $n = 412$ SC cords from 8 maraviroc-treated mice).

Data are presented as mean \pm SEM. For (C)–(E), an unpaired two-tailed Student's t test was used. For (G), an unpaired two-tailed Welch's t test was used.

* $p < 0.05$; ** $p < 0.01$; *** $p < 0.001$; ns, not significant.

See also Figure S5.



(legend on next page)

In summary, we have identified a novel role for CCL3 as a chemotactic factor directing collective SC migration and aiding nerve regeneration. These findings increase further our understanding of the complex multicellular response required to regenerate new nerve tissue in the adult and provides a potential new therapeutic target to both improve nerve repair and inhibit aberrant nerve regeneration processes.

Limitations of the study

Our data clearly show that CCL3 inhibition blocks efficient nerve regeneration. However, the CCL3 KO mouse was a complete KO; we therefore do not know whether other cell types, such as neutrophils, contribute to the expression of CCL3 at the site of injury. Our work indicates a possible mechanism for CCL3 in neuroma formation, based on structural similarities resulting from a failure of the regenerative process.³⁸ Future studies could determine the role of the CCL3/CCR1/5 axis in the formation and sustainment of these pathologies and whether targeting this pathway represents a promising therapeutic approach.

RESOURCE AVAILABILITY

Lead contact

Further information and requests for resources and reagents should be directed to and will be fulfilled by the lead contact, Alison Lloyd (alison.lloyd@ucl.ac.uk).

Materials availability

This study did not generate new unique reagents.

Data and code availability

- All data reported in this paper will be shared by the [lead contact](#) upon request.
- Any additional information required to reanalyze the data reported in this paper is available from the [lead contact](#) upon request.
- This study did not generate/analyze datasets/code.

ACKNOWLEDGMENTS

This work was supported by a program grant from Cancer Research UK (C378/A4308), the Rosetrees Trust, and MRC and UCL Repurposing TIN Pilot Data Fund (grant no. 178973). We would like to thank UCL Biological Services for animal husbandry and useful advice; Prof. Mark Marsh for providing us with the THP-1 cells; and the Lloyd lab for advice, assistance with surgeries, and useful discussions.

Figure 6. CCL3 ablation impairs nerve regeneration and leads to aberrant nerve growth

- (A) Representative confocal images of longitudinal sections from control and CCL3 KO mice, 90 days after sciatic nerve injury, SCs are visualized with eGFP (green, PLP-eGFP mice) and immunostained to detect axons (NF, white), with nuclei stained with Hoechst (blue). Arrow indicates the proximal (P) to distal (D) direction. White dashed lines indicate the regenerated region that forms from the nerve bridge. Yellow dashed lines indicate aberrant regions only seen in CCL3 KO nerves. Scale bar, 300 µm.
- (B) Magnified images of (A), showing the polarization of axonal regrowth in the regenerated and aberrant regions. Scale bar, 50 µm.
- (C) Quantification of the total area, SC area, and axonal area of regenerated regions of control and CCL3 KO mice ($n = 5$ control mice; $n = 6$ CCL3 KO mice).
- (D) Quantification of the angle of deviation from the vertical of axons in regenerated and aberrant areas of control and CCL3 KO mice ($n = 210$ axons, regenerated region from 5 control mice; $n = 249$ axons, regenerated region from 6 CCL3 KO mice; $n = 224$ axons, aberrant region from 6 CCL3 KO mice).
- (E) Representative confocal images of longitudinal sections immunostained to detect axons (NF, white) in the distal stump of control and CCL3 KO mice. Scale bar, 100 µm.
- (F) Quantification of (E) ($n = 5$ control mice; $n = 5$ CCL3 KO mice).
- (G) Quantification of the aberrant region in control and CCL3 KO mice ($n = 5$ control mice; $n = 6$ CCL3 KO mice).

Data are presented as mean ± SEM. For (C), (F), and (G), an unpaired two-tailed Student's t test was used. For (D), a one-way ANOVA test was used. * $p < 0.05$; ** $p < 0.01$; *** $p < 0.0001$; ns, not significant.

See also [Figure S6](#).

AUTHOR CONTRIBUTIONS

A.C.L. conceived the project. L.V.E. and G.M.-C. performed the majority of the experiments, with help from E.H.-W., A.-L.C., A.P., I.B.-C., G.C., and I.J.W. E.H.-W., A.-L.C., and C.L.B. advised on the experimental design. A.C.L. supervised the study. L.V.E., G.M.-C., E.H.-W., and A.C.L. interpreted the data and wrote the manuscript. All authors discussed the results and commented on the manuscript.

DECLARATION OF INTERESTS

The authors declare no competing interests.

STAR METHODS

Detailed methods are provided in the online version of this paper and include the following:

- **KEY RESOURCES TABLE**
- **EXPERIMENTAL MODEL AND STUDY PARTICIPANT DETAILS**
 - Animal studies
- **METHOD DETAILS**
 - Sciatic nerve injury
 - Cell culture
 - Ex-vivo bridge cell isolation and culture
 - NSΔRafER SCs differentiation assays
 - Macrophage cell line hypoxia assays
 - Boyden chamber migration assay
 - Dunn chamber migration assay
 - Proliferation assay
 - Short interfering RNA knockdown
 - RNA extraction and RTqPCR
 - Primers sequences
 - RNA-seq data analysis
 - Protein extraction from cell supernatant
 - Western blot analysis
 - Immunofluorescence
 - Immunofluorescence antibodies
 - Image analysis
 - Electron microscopy
- **QUANTIFICATION AND STATISTICAL ANALYSIS**

SUPPLEMENTAL INFORMATION

Supplemental information can be found online at <https://doi.org/10.1016/j.celrep.2025.115322>.

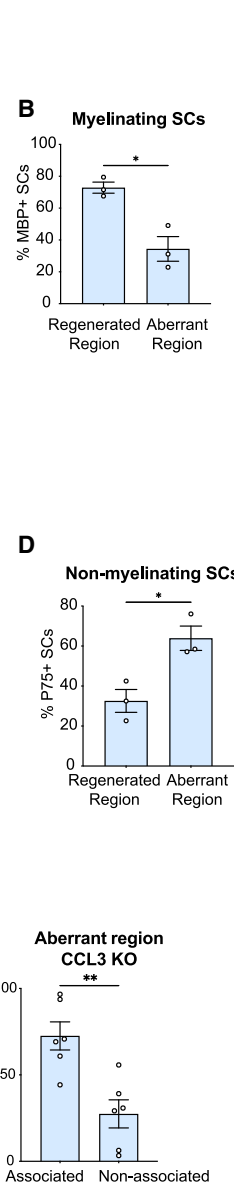
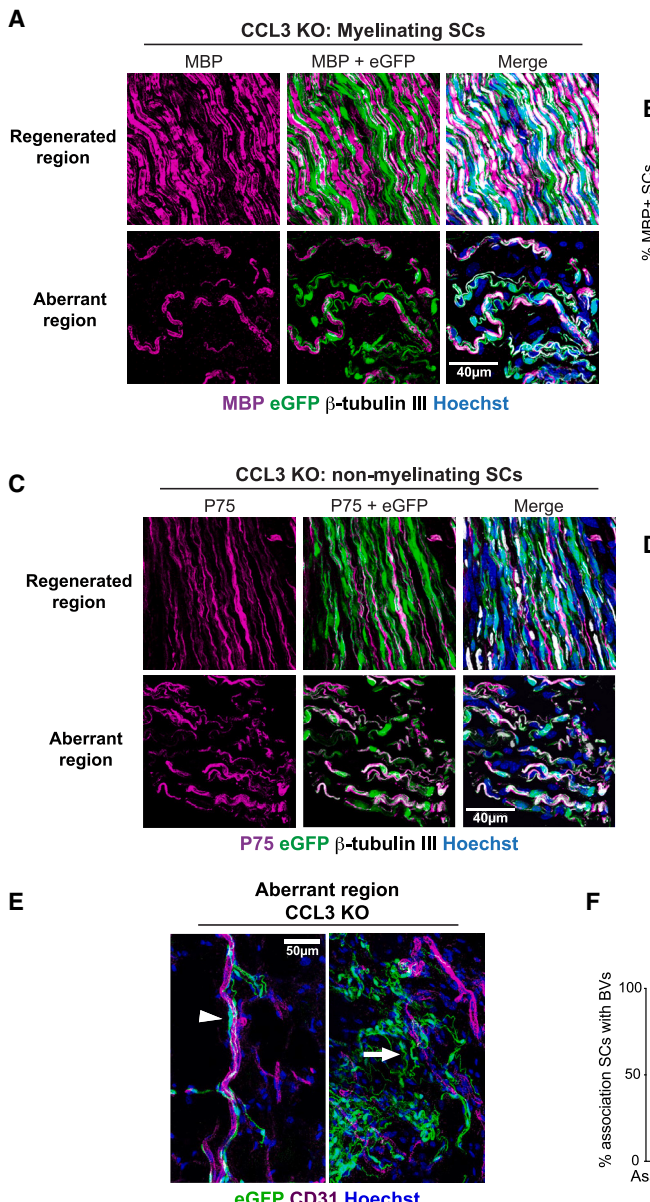


Figure 7. Schwann cells remain undifferentiated in aberrant regions following nerve injury

(A) Representative confocal images of CCL3 KO mice nerves at Day 90 after transection, showing myelin expression (MBP, magenta) in SCs (eGFP, green) in aberrant and regenerated regions. Sections were also immunostained to detect axons (β -tubulin III, white), and nuclei were stained with Hoechst (blue) ($n = 3$ CCL3 KO mice). Scale bar, 40 μ m.

(B) Quantification of (A). Data are presented as mean \pm SEM.

(C) Representative images of CCL3 KO mice nerves at Day 90 after transection, to detect non-myelinating SCs (p75, magenta) in aberrant and regenerated regions. SCs were detected by expression of eGFP (green), and sections were also immunostained to detect axons (β -tubulin III, white); nuclei were stained with Hoechst (blue) ($n = 3$ CCL3 KO mice). Scale bar, 40 μ m.

(D) Quantification of (C). Data are presented as mean \pm SEM.

(E) Representative confocal images of the aberrant regions of CCL3 KO mice showing SCs (eGFP, green) and immunostained to detect endothelial cells (CD31, magenta). Arrowhead indicates an example of an SC interacting with a blood vessel (BV). Arrow indicates an SC independent of detectable BV association. Scale bar, 50 μ m.

(F) Quantification of SCs associated or not associated with BVs in aberrant regions ($n = 6$ CCL3 KO mice).

For (B), (D), and (F), an unpaired two-tailed Student's t test was used. * $p < 0.05$; ** $p < 0.01$.

Received: September 11, 2024
Revised: December 14, 2024
Accepted: January 27, 2025
Published: February 16, 2025

REFERENCES

1. Aguayo, A.J., David, S., and Bray, G.M. (1981). Influences of the Glial Environment on the Elongation of Axons after Injury - Transplantation Studies in Adult Rodents. *J. Exp. Biol.* 95, 231–240.
2. Brosius Lutz, A., and Barres, B.A. (2014). Contrasting the glial response to axon injury in the central and peripheral nervous systems. *Dev. Cell* 28, 7–17. <https://doi.org/10.1016/j.devcel.2013.12.002>.
3. Zochodne, D.W. (2012). The challenges and beauty of peripheral nerve regeneration. *J. Peripher. Nerv. Syst.* 17, 1–18. <https://doi.org/10.1111/j.1529-8027.2012.00378.x>.
4. Cattin, A.L., and Lloyd, A.C. (2016). The multicellular complexity of peripheral nerve regeneration. *Curr. Opin. Neurobiol.* 39, 38–46. <https://doi.org/10.1016/j.conb.2016.04.005>.
5. Jurecka, W., Ammerer, H.P., and Lassmann, H. (1975). Regeneration of a transected peripheral nerve. An autoradiographic and electron microscopic study. *Acta Neuropathol.* 32, 299–312. <https://doi.org/10.1007/BF00696792>.
6. Grinsell, D., and Keating, C.P. (2014). Peripheral nerve reconstruction after injury: a review of clinical and experimental therapies. *BioMed Res. Int.* 2014, 698256. <https://doi.org/10.1155/2014/698256>.
7. Houschyar, K.S., Momeni, A., Pyles, M.N., Cha, J.Y., Maan, Z.N., Duscher, D., Jew, O.S., Siemers, F., and van Schoonhoven, J. (2016). The Role of Current Techniques and Concepts in Peripheral Nerve Repair. *Plast. Surg. Int.* 2016, 4175293. <https://doi.org/10.1155/2016/4175293>.

8. Barnes, S.L., Miller, T.A., and Simon, N.G. (2022). Traumatic peripheral nerve injuries: diagnosis and management. *Curr. Opin. Neurol.* 35, 718–727. <https://doi.org/10.1097/WCO.0000000000001116>.
9. Costigan, M., Scholz, J., and Woolf, C.J. (2009). Neuropathic pain: a mal-adaptive response of the nervous system to damage. *Annu. Rev. Neurosci.* 32, 1–32. <https://doi.org/10.1146/annurev.neuro.051508.135531>.
10. Stassart, R.M., Gomez-Sanchez, J.A., and Lloyd, A.C. (2024). Schwann Cells as Orchestrators of Nerve Repair: Implications for Tissue Regeneration and Pathologies. *Cold Spring Harbor Perspect. Biol.* 16, a041363. <https://doi.org/10.1101/cshperspect.a041363>.
11. Jessen, K.R., and Mirsky, R. (2019). The Success and Failure of the Schwann Cell Response to Nerve Injury. *Front. Cell. Neurosci.* 13, 33. <https://doi.org/10.3389/fncel.2019.00033>.
12. Napoli, I., Noon, L.A., Ribeiro, S., Kerai, A.P., Parrinello, S., Rosenberg, L.H., Collins, M.J., Harris, M.C., White, I.J., Woodhoo, A., and Lloyd, A.C. (2012). A central role for the ERK-signaling pathway in controlling Schwann cell plasticity and peripheral nerve regeneration in vivo. *Neuron* 73, 729–742. <https://doi.org/10.1016/j.neuron.2011.11.031>.
13. Stierli, S., Imperatore, V., and Lloyd, A.C. (2019). Schwann cell plasticity—roles in tissue homeostasis, regeneration, and disease. *Glia* 67, 2203–2215. <https://doi.org/10.1002/glia.23643>.
14. Cattin, A.L., Burden, J.J., Van Emmenis, L., Mackenzie, F.E., Hoving, J.J.A., Garcia Calavia, N., Guo, Y., McLaughlin, M., Rosenberg, L.H., Quereda, V., et al. (2015). Macrophage-Induced Blood Vessels Guide Schwann Cell-Mediated Regeneration of Peripheral Nerves. *Cell* 162, 1127–1139. <https://doi.org/10.1016/j.cell.2015.07.021>.
15. Parrinello, S., Napoli, I., Ribeiro, S., Wingfield Digby, P., Fedorova, M., Parkinson, D.B., Doddrell, R.D.S., Nakayama, M., Adams, R.H., and Lloyd, A.C. (2010). EphB signaling directs peripheral nerve regeneration through Sox2-dependent Schwann cell sorting. *Cell* 143, 145–155. <https://doi.org/10.1016/j.cell.2010.08.039>.
16. Stramer, B., and Mayor, R. (2017). Mechanisms and in vivo functions of contact inhibition of locomotion. *Nat. Rev. Mol. Cell Biol.* 18, 43–55. <https://doi.org/10.1038/nrm.2016.118>.
17. Hoving, J.J.A., Harford-Wright, E., Wingfield-Digby, P., Cattin, A.L., Campana, M., Power, A., Morgan, T., Torchiaro, E., Quereda, V., and Lloyd, A.C. (2024). N-cadherin directs the collective Schwann cell migration required for nerve regeneration through Slit2/3 mediated contact inhibition of locomotion. *Elife* 13, e88872. <https://doi.org/10.7554/elife.88872>.
18. Friedl, P., and Gilmour, D. (2009). Collective cell migration in morphogenesis, regeneration and cancer. *Nat. Rev. Mol. Cell Biol.* 10, 445–457. <https://doi.org/10.1038/nrm2720>.
19. Mishra, A.K., Campanale, J.P., Mondo, J.A., and Montell, D.J. (2019). Cell interactions in collective cell migration. *Development* 146, dev172056. <https://doi.org/10.1242/dev.172056>.
20. Rorth, P. (2009). Collective cell migration. *Annu. Rev. Cell Dev. Biol.* 25, 407–429. <https://doi.org/10.1146/annurev.cellbio.042308.113231>.
21. Stehbens, S.J., Scarpa, E., and White, M.D. (2024). Perspectives in collective cell migration - moving forward. *J. Cell Sci.* 137, jcs261549. <https://doi.org/10.1242/jcs.261549>.
22. Mayor, R., and Carmona-Fontaine, C. (2010). Keeping in touch with contact inhibition of locomotion. *Trends Cell Biol.* 20, 319–328. <https://doi.org/10.1016/j.tcb.2010.03.005>.
23. SenGupta, S., Parent, C.A., and Bear, J.E. (2021). The principles of directed cell migration. *Nat. Rev. Mol. Cell Biol.* 22, 529–547. <https://doi.org/10.1038/s41580-021-00366-6>.
24. Shellard, A., and Mayor, R. (2020). All Roads Lead to Directional Cell Migration. *Trends Cell Biol.* 30, 852–868. <https://doi.org/10.1016/j.tcb.2020.08.002>.
25. Shellard, A., and Mayor, R. (2016). Chemotaxis during neural crest migration. *Semin. Cell Dev. Biol.* 55, 111–118. <https://doi.org/10.1016/j.semcd.2016.01.031>.
26. Szabo, A., and Mayor, R. (2018). Mechanisms of Neural Crest Migration. *Annu. Rev. Genet.* 52, 43–63. <https://doi.org/10.1146/annurev-genet-120417-031559>.
27. Theveneau, E., Steventon, B., Scarpa, E., Garcia, S., Trepat, X., Streit, A., and Mayor, R. (2013). Chase-and-run between adjacent cell populations promotes directional collective migration. *Nat. Cell Biol.* 15, 763–772. <https://doi.org/10.1038/ncb2772>.
28. Clements, M.P., Byrne, E., Camarillo Guerrero, L.F., Cattin, A.L., Zakka, L., Ashraf, A., Burden, J.J., Khadayate, S., Lloyd, A.C., Marguerat, S., and Parrinello, S. (2017). The Wound Microenvironment Reprograms Schwann Cells to Invasive Mesenchymal-like Cells to Drive Peripheral Nerve Regeneration. *Neuron* 96, 98–114.e7. <https://doi.org/10.1016/j.neuron.2017.09.008>.
29. Dorr, P., Westby, M., Dobbs, S., Griffin, P., Irvine, B., Macartney, M., Mori, J., Rickett, G., Smith-Burchell, C., Napier, C., et al. (2005). Maraviroc (UK-427,857), a potent, orally bioavailable, and selective small-molecule inhibitor of chemokine receptor CCR5 with broad-spectrum anti-human immunodeficiency virus type 1 activity. *Antimicrob. Agents Chemother.* 49, 4721–4732. <https://doi.org/10.1128/AAC.49.11.4721-4732.2005>.
30. Sabroe, I., Peck, M.J., Van Keulen, B.J., Jorritsma, A., Simmons, G., Clapham, P.R., Williams, T.J., and Pease, J.E. (2000). A small molecule antagonist of chemokine receptors CCR1 and CCR3. Potent inhibition of eosinophil function and CCR3-mediated HIV-1 entry. *J. Biol. Chem.* 275, 25985–25992. <https://doi.org/10.1074/jbc.M908864199>.
31. Kramp, B.K., Megens, R.T.A., Sarabi, A., Winkler, S., Projahn, D., Weber, C., Koenen, R.R., and von Hundelshausen, P. (2013). Exchange of extracellular domains of CCR1 and CCR5 reveals confined functions in CCL5-mediated cell recruitment. *Thromb. Haemostasis* 110, 795–806. <https://doi.org/10.1160/TH13-05-0420>.
32. Choi, H.M.T., Calvert, C.R., Husain, N., Huss, D., Barsi, J.C., Deverman, B.E., Hunter, R.C., Kato, M., Lee, S.M., Abelin, A.C.T., et al. (2016). Mapping a multiplexed zoo of mRNA expression. *Development* 143, 3632–3637. <https://doi.org/10.1242/dev.140137>.
33. Schwarzkopf, M., Liu, M.C., Schulte, S.J., Ives, R., Husain, N., Choi, H.M.T., and Pierce, N.A. (2021). Hybridization chain reaction enables a unified approach to multiplexed, quantitative, high-resolution immunohistochemistry and *in situ* hybridization. *Development* 148, dev199847. <https://doi.org/10.1242/dev.199847>.
34. Cook, D.N., Beck, M.A., Coffman, T.M., Kirby, S.L., Sheridan, J.F., Pragnell, I.B., and Smithies, O. (1995). Requirement of MIP-1 alpha for an inflammatory response to viral infection. *Science* 269, 1583–1585. <https://doi.org/10.1126/science.7667639>.
35. Mallon, B.S., Shick, H.E., Kidd, G.J., and Macklin, W.B. (2002). Proteolipid promoter activity distinguishes two populations of NG2-positive cells throughout neonatal cortical development. *J. Neurosci.* 22, 876–885. <https://doi.org/10.1523/JNEUROSCI.22-03-00876.2002>.
36. Lassmann, H., Jurecka, W., and Gebhart, W. (1976). Some electron microscopic and autoradiographic results concerning cutaneous neurofibromas in von Recklinghausen's disease. *Arch. Dermatol. Res.* (1975) 255, 69–81. <https://doi.org/10.1007/BF00581680>.
37. Lu, C., Sun, X., Wang, C., Wang, Y., and Peng, J. (2018). Mechanisms and treatment of painful neuromas. *Rev. Neurosci.* 29, 557–566. <https://doi.org/10.1515/revneuro-2017-0077>.
38. Deininger, S., Schumacher, J., Blechschmidt, A., Song, J., Klugmann, C., Antoniadis, G., Pedro, M., Knöll, B., and Meyer Zu Reckendorf, S. (2024). Nerve injury converts Schwann cells in a long-term repair-like state in human neuroma tissue. *Exp. Neurol.* 382, 114981. <https://doi.org/10.1016/j.expneurol.2024.114981>.
39. Perrin, F.E., Lacroix, S., Avilés-Trigueros, M., and David, S. (2005). Involvement of monocyte chemoattractant protein-1, macrophage inflammatory protein-1alpha and interleukin-1beta in Wallerian degeneration. *Brain* 128, 854–866. <https://doi.org/10.1093/brain/awh407>.
40. Taskinen, H.S., and Röyttä, M. (2000). Increased expression of chemokines (MCP-1, MIP-1alpha, RANTES) after peripheral nerve transection.

- J. Peripher. Nerv. Syst. 5, 75–81. <https://doi.org/10.1046/j.1529-8027.2000.00009.x>.
41. Woollard, S.M., and Kanmogne, G.D. (2015). Maraviroc: a review of its use in HIV infection and beyond. Drug Des. Dev. Ther. 9, 5447–5468. <https://doi.org/10.2147/DDDT.S90580>.
42. Jiao, X., Nawab, O., Patel, T., Kossenkov, A.V., Halama, N., Jaeger, D., and Pestell, R.G. (2019). Recent Advances Targeting CCR5 for Cancer and Its Role in Immuno-Oncology. Cancer Res. 79, 4801–4807. <https://doi.org/10.1158/0008-5472.CAN-19-1167>.
43. Salonen, V., Aho, H., Röyttä, M., and Peltonen, J. (1988). Quantitation of Schwann cells and endoneurial fibroblast-like cells after experimental nerve trauma. Acta Neuropathol. 75, 331–336. <https://doi.org/10.1007/BF00687785>.
44. Stierli, S., Napoli, I., White, I.J., Cattin, A.L., Monteza Cabrejos, A., Garcia Calavia, N., Malong, L., Ribeiro, S., Nihouarn, J., Williams, R., et al. (2018). The regulation of the homeostasis and regeneration of peripheral nerve is distinct from the CNS and independent of a stem cell population. Development 145, dev170316. <https://doi.org/10.1242/dev.170316>.
45. Abreu, E., Aubert, S., Wavreille, G., Gheno, R., Canella, C., and Cotten, A. (2013). Peripheral tumor and tumor-like neurogenic lesions. Eur. J. Radiol. 82, 38–50. <https://doi.org/10.1016/j.ejrad.2011.04.036>.
46. Camley, B.A., Zimmermann, J., Levine, H., and Rappel, W.J. (2016). Emergent Collective Chemotaxis without Single-Cell Gradient Sensing. Phys. Rev. Lett. 116, 098101. <https://doi.org/10.1103/PhysRevLett.116.098101>.
47. Malet-Engra, G., Yu, W., Oldani, A., Rey-Barroso, J., Gov, N.S., Scita, G., and Dupré, L. (2015). Collective cell motility promotes chemotactic prowess and resistance to chemorepulsion. Curr. Biol. 25, 242–250. <https://doi.org/10.1016/j.cub.2014.11.030>.
48. Shellard, A., and Mayor, R. (2020). Rules of collective migration: from the wildebeest to the neural crest. Philos. Trans. R. Soc. Lond. B Biol. Sci. 375, 20190387. <https://doi.org/10.1098/rstb.2019.0387>.
49. Carmona-Fontaine, C., Theveneau, E., Tzekou, A., Tada, M., Woods, M., Page, K.M., Parsons, M., Lambiris, J.D., and Mayor, R. (2011). Complement fragment C3a controls mutual cell attraction during collective cell migration. Dev. Cell 21, 1026–1037. <https://doi.org/10.1016/j.devcel.2011.10.012>.
50. Woods, M.L., Carmona-Fontaine, C., Barnes, C.P., Couzin, I.D., Mayor, R., and Page, K.M. (2014). Directional collective cell migration emerges as a property of cell interactions. PLoS One 9, e104969. <https://doi.org/10.1371/journal.pone.0104969>.
51. Jessen, K.R., and Mirsky, R. (2019). Schwann Cell Precursors: Multipotent Glial Cells in Embryonic Nerves. Front. Mol. Neurosci. 12, 69. <https://doi.org/10.3389/fnmol.2019.00069>.
52. Perlin, J.R., Lush, M.E., Stephens, W.Z., Piotrowski, T., and Talbot, W.S. (2011). Neuronal Neuregulin 1 type III directs Schwann cell migration. Development 138, 4639–4648. <https://doi.org/10.1242/dev.068072>.
53. Monje, M., Borniger, J.C., D'Silva, N.J., Deneen, B., Dirks, P.B., Fattah, F., Frenette, P.S., Garzia, L., Gutmann, D.H., Hanahan, D., et al. (2020). Roadmap for the Emerging Field of Cancer Neuroscience. Cell 181, 219–222. <https://doi.org/10.1016/j.cell.2020.03.034>.
54. Schindelin, J., Arganda-Carreras, I., Frise, E., Kaynig, V., Longair, M., Pietzsch, T., Preibisch, S., Rueden, C., Saalfeld, S., Schmid, B., et al. (2012). Fiji: an open-source platform for biological-image analysis. Nat. Methods 9, 676–682. <https://doi.org/10.1038/nmeth.2019>.
55. Halvorsen, E.C., Hamilton, M.J., Young, A., Wadsworth, B.J., LePard, N.E., Lee, H.N., Firmino, N., Collier, J.L., and Bennewith, K.L. (2016). Maraviroc decreases CCL8-mediated migration of CCR5(+) regulatory T cells and reduces metastatic tumor growth in the lungs. Oncoimmunology 5, e1150398. <https://doi.org/10.1080/2162402X.2016.1150398>.
56. Mathon, N.F., Malcolm, D.S., Harris, M.C., Cheng, L., and Lloyd, A.C. (2001). Lack of replicative senescence in normal rodent glia. Science 291, 872–875. <https://doi.org/10.1126/science.1056782>.
57. Harris, M.C., Perez-Nadale, E., Parkinson, D.B., Malcolm, D.S., Mudge, A.W., and Lloyd, A.C. (2004). The Ras/Raf/ERK signalling pathway drives Schwann cell dedifferentiation. EMBO J. 23, 3061–3071. <https://doi.org/10.1038/sj.emboj.7600309>.
58. Zicha, D., Dunn, G.A., and Brown, A.F. (1991). A new direct-viewing chemotaxis chamber. J. Cell Sci. 99, 769–775. <https://doi.org/10.1242/jcs.99.4.769>.
59. Gorelik, R., and Gautreau, A. (2014). Quantitative and unbiased analysis of directional persistence in cell migration. Nat. Protoc. 9, 1931–1943. <https://doi.org/10.1038/nprot.2014.131>.

STAR★METHODS

KEY RESOURCES TABLE

REAGENT or RESOURCE	SOURCE	IDENTIFIER
Antibodies		
Chicken polyclonal anti- 200kD neurofilament	Abcam	Cat#ab4680;RRID:AB_30456
Rat Anti-Mouse CD31	BD Pharmingen	Cat#553370;RRID:AB_396660
Rat F4/80 monoclonal (clone Cl:A3-1) Bio-Rad Cat#MCA497	Bio-Rad	Cat# MCA497;RRID:AB_2098196
Rabbit Glut1 polyclonal	Abcam	Cat#ab652;RRID:AB_305540
Rabbit Iba1 polyclonal	Wako	Cat#019-19741;RRID:AB_839504
Goat CD31/PECAM-1 Antibody	R & D Systems	Cat#AF3628;RRID:AB_2161028
Rabbit S100	Dako (Agilent)	Cat#Z0311;RRID:AB_10013383
anti-Tubulin β-3 (TUBB3)	Biolegend	Cat#802001; RRID:AB_2564645
Mouse Anti-Prolyl-4-Hydroxylase beta	Origene	Cat# AF5110-1; RRID:AB_1006633
Anti-Macrophage Inflammatory Protein 1 alpha (CCL3)	Abcam	Cat#ab25128; RRID:AB_448640
β-actin	Abcam	Cat#ab8227; RRID:AB_2305186
Anti-rabbit IgG, HRP-linked Antibody	Cell Signaling	Cat#7074P2; RRID:AB_2099233
Polyclonal Rabbit anti-mouse IgG	Dako (Agilent)	Cat#Z0259; RRID:AB_2532147
Purified Mouse Anti-Rat CD11b/c	BD Biosciences	Cat#554859; RRID:AB_395560
Thy1 clone Ox7	In house	N/A
Anti-MBP	Thermo Fisher Scientific	Cat#PA1-10008; RRID:AB_1077024
Anti-p75NTR	EMD Millipore	Cat#07-476; RRID:AB_310649
Goat anti-Chicken Alexa Fluor 647	Thermo Fisher Scientific	Cat#A21449; RRID:AB_2535866
Goat anti-Rat Alexa Fluor 594	Thermo Fisher Scientific	Cat#A11007; RRID:AB_10561522
Donkey anti-Rat Alexa Fluor 647	Abcam	Cat#ab150155; RRID:AB_2813835
Donkey anti-Rabbit Alexa Fluor 594	Thermo Fisher Scientific	Cat#A21207; RRID:AB_141637
Donkey anti-Goat Alexa Fluor 594	Thermo Fisher Scientific	Cat#A11058; RRID:AB_2534105
Donkey anti-Rabbit Alexa Fluor 488	Thermo Fisher Scientific	Cat#A21206; RRID:AB_2535792
Donkey anti-Rabbit Alexa Fluor 647	Thermo Fisher Scientific	Cat#A31573; RRID:AB_2536183
Goat anti-Mouse Alexa Fluor 488	Thermo Fisher Scientific	Cat#A11001; RRID:AB_2534069
Goat anti-Rabbit Alexa Fluor 594	Thermo Fisher Scientific	Cat#A11012; RRID:AB_2534079
HCR™ Amplifiers B3-647	Molecular instruments	HCR™
HCR™ Amplifiers B2-594	Molecular instruments	HCR™
Chemicals, peptides, and recombinant proteins		
Goat Serum	Sigma-Aldrich	G9023
Donkey serum	Sigma-Aldrich	D9663
Formaldehyde 16%	TAAB Laboratories	F017
Recombinant Rat CCL3/MIP-1 alpha Protein	R&D Systems	6625-MA-025
Recombinant Human CCL3/MIP-1 alpha Protein	R&D Systems	270-LD-010/CF

(Continued on next page)

Continued

REAGENT or RESOURCE	SOURCE	IDENTIFIER
Maraviroc	BioTechne	3756
DMSO	Tocris	3176
DPBS	ThermoFisher	14190169
Poly-L-lysine (PLL)	Sigma-Aldrich	P1274-25MG
Fetal Bovine Serum (FBS)	BioSera	FB-1001/500
L-Glutamine	ThermoFisher	25030-081
Forskolin	Abcam	ab120058
Kanamycin	ThermoFisher	11815-032
Gentamycin	ThermoFisher	15710049
Glial Growth Factor (GGF)	Produced in lab	N/A
Bovine Serum Albumin (BSA)	Sigma-Aldrich	A3294
Trizol	ThermoFisher	15596018
Fibronectin	Sigma-Aldrich	F1141
Hoechst	Sigma-Aldrich	94403
Laminin	Sigma-Aldrich	L2020
Trichloroacetic acid	Sigma-Aldrich	T6399
Acetone	VWR	20066.310P
Laemmli buffer	Biorad	1610747
β-mercaptoethanol	Sigma-Aldrich	M3148
Pierce-ECL western blot substrate	ThermoFisher	32106
Luminata Crescendo Western HRP substrate	EMD-Millipore	ELLUR
Sucrose	Sigma-Aldrich	S0389
OCT	VWR	361603E
DAPI	Sigma-Aldrich	D9542-5MG
Fluoromount G	ThermoFisher	00-4958-02
DEPC-Treated Water	ThermoFisher	AM9922
Ethanol	Sigma-Aldrich	32221
Hybridisation buffer	Molecular instruments	HCR™
Probe wash buffer	Molecular instruments	HCR™
Amplification Buffer	Molecular instruments	HCR™
SSC 20X	ThermoFisher	AM9763
Glutaraldehyde (EM grade) 20%	TAAB Laboratories	G011
Osmium Tetroxide 2% aqueous	TAAB Laboratories	0005
HiPerFect Transfection Reagent	Qiagen	301704
PBS - Phosphate-Buffered Saline (10X)	ThermoFisher	AM9625
N,6'2'-O-Dibutyryladenosine 3',5'-cyclic monophosphate sodium salt (dbcAMP)	Sigma-Aldrich	D0260-5MG
Hydroxytamoxifen	Sigma-Aldrich	T-5648
IGF-1 human recombinant	Source BioScience	ABE1368
Recombinant Human NRG1-beta 1/HRG1-beta 1	R&D Systems	377-HB-050
ECD Protein (NRG1)		

Critical commercial assays

MESA Blue qPCR Mastermix Plus Kit	Eurogentec	RT-SY2X03+NRWOU8
SuperScript II	Thermo Fisher Scientific	18064014
SuperScript IV	Thermo Fisher Scientific	18090010
Hypoxyprobe™ kit	Hypoxyprobe	HP1-100kit
Mouse Cytokine Array Panel A	R&D Systems	ARY006
PureLink RNA Micro kit	Thermo Fisher Scientific	Cat#12183016
Click-iT® EdU Alexa Fluor 647 kit	Thermo Fisher Scientific	C10340

(Continued on next page)

Continued

REAGENT or RESOURCE	SOURCE	IDENTIFIER
Experimental models: Cell lines		
THP-1 cell line	Prof. Mark Marsh laboratory	N/A
J774A.1 mouse macrophage cell line	Sigma-Aldrich	Cat: 91051511
Experimental models: Organisms/strains		
B6; CBA-Tg(Plp1-EGFP)10Wmac/J mice (Mallon et al. ³⁵)	Cattin et al. ¹⁴	Cattin et al. ¹⁴ Strain# 033357; RRID:IMSR_JAX:033357
B6.129P2-Ccl3 ^{tm1Unc} /J (CCL3 KO) mice	The Jackson Laboratory	Strain #:002687; RRID:IMSR_JAX:002687
PLP-eGFP-CCL3 KO mice	This paper	N/A
Sprague-Dawley rats	Charles River Laboratories	001 Cat#734476; RRID:RGD734476
Oligonucleotides		
Rat CCL3: Fwd: 5'- CCATATGGAGCTGACACCCCC-3' Rev: 5'- TCTGCCGGTTCTTGGTC-3'	This Paper	N/A
Mouse CCL3: Fwd: 5'- CCATATGGAGCTGACACCCCC-3' Rev: 5'- AAATGACACCTGGCTGGGAG-3'	This Paper	N/A
Human CCL3: Fwd: 5'- ACATTCCGTACACTGCTCAG -3' Rev: 5'- TTGTTGCCAACAGGCCACAC-3'	This Paper	N/A
Rat CCR1: Fwd: 5'- CAAAGGCCAGAAACAAGCC-3' Rev: 5'- AGCCCCGAAGGCTTACAT-3'	This Paper	N/A
Human CCR1: Fwd: 5'- GGTCCCTGGCCTTGCAAT-3' Rev: 5'- AGGGAAGCGTGAACAGGAAG-3'	This Paper	N/A
CCL3 siRNA 1: 5'-CTAGGTAGACATGATGACAAA-3'	This Paper	N/A
CCL3 siRNA 3: 5'-TCGAGGGACTCTTCACTTGAA-3'	This Paper	N/A
CCR1 siRNA: 5'-CAGACCCTAGGTGTCACCAA-3'	This Paper	N/A
Scr: 5'-AATTCTCCGAACGTGTCACGT-3'	This Paper	N/A
HCR™ CCL3-B3 probes set	Molecular instruments	HCR™
HCR™ CCR2-B2 probes set	Molecular instruments	HCR™
Software and algorithms		
Fiji/ImageJ	Schindelin et al. ⁵⁴	https://imagej.net/Fiji/Downloads
Prism	GraphPad	https://www.graphpad.com/scientificsoftware/prism
Adobe Photoshop CC	Adobe Systems	https://www.adobe.com
Adobe Illustrator CC	Adobe Systems	https://www.adobe.com
Velocity	Improvision	https://www.velocity4d.com/
Other		
SPE3	Leica TCS SPE	405nm, 488nm, 561nm and 635nm
SPE8	Leica TCS SPE8 STED 3x	405nm, 488nm, 561nm and 635nm
LSM900	Zeiss LSM900	405, 488, 561 and 640 lasers
Transmission electron microscope (TEM)	FEI Tecnai 12 Spirit BioTwin	OSIS morada
Axiovert 200M	Zeiss Axiovert 200M	Phase contrast (Transmitted light microscopy)
Axio Imager.A1	Zeiss Axio Imager.A1	405nm
Subio X Omics	Subio Platform	https://www.subioplatform.com/
Other		
RNA-Seq raw and analyzed data	Clements et al. ²⁸	GEO: GSE103039

EXPERIMENTAL MODEL AND STUDY PARTICIPANT DETAILS

Animal studies

Animal work was carried out in accordance with UK Home Office regulations in the Biological Services Central Facility at University College London and was approved by the UCL Animal Welfare and Ethical Review Body. Mice and rats were group housed with free access to food and water, in a temperature-controlled room (20°C–24°C, 45–64% humidity) on a 12-h light/dark cycle. Adult male (6–8-week-old) Sprague-Dawley rats were used, weighing between (250–500g). PLP-eGFP transgenic mice³⁵ were crossed with CCL3 KO mice acquired from The Jackson Laboratory. Both male and female mice (8–12 weeks old) were used, and animals were randomly assigned to each experimental group. Primary rat SCs were isolated from the nerves of postnatal Day 7 male and female Sprague-Dawley rats. Human SCs were acquired from ScienCell. The J774A.1 mouse macrophage cell line was purchased from Sigma. Cells were routinely tested for mycoplasma contamination.

METHOD DETAILS

Sciatic nerve injury

Sciatic nerve injury was performed under aseptic conditions by exposing the right sciatic nerves of animals under isoflurane anesthetic, with a full or half cut performed by transecting the nerve at mid-thigh. The wound was closed with surgical clips and the animal allowed to recover, with nerves harvested at the indicated time points for analysis. Note, following a full transection, the vast majority of nerve stumps re-join to form a nerve bridge, with no interventions. We find close to 100% efficiency in rats, with greater than 95% efficiency in mice.

For injection experiments, on Day 2 following half transections in rats, nerves were re-exposed under isoflurane anesthetic and each bridge was injected with 5µl of vehicle (PBS) or recombinant CCL3 (R&D Systems, 50 µg/ml) using a hand-held glass capillary coupled to a Hamilton syringe mounted to a microinjector (Sutter Instrument). The wound was subsequently reclosed with sutures, the animal allowed to recover, and nerves harvested at Day 6 post-injury for analysis.

To test the effect of CCR5 inhibition after nerve injury, PLP-eGFP mice were administered with maraviroc (BioTechne, 25 mg/kg) diluted in 5% DMSO in water or vehicle orally every 12 h, from Days 5–7 post-injury. This dose has previously been shown to be effective and non-toxic in mice.⁵⁵ Sciatic nerves were collected at Day 7 to perform immunostaining analysis.

Cell culture

Primary rat SCs were isolated from the nerves of postnatal Day 7 Sprague-Dawley rats, as previously described.⁵⁶ SCs were cultured on poly-L-lysine (PLL)-coated plates in Dulbecco's Modified Eagle's Medium (low glucose, 1 g/l) (DMEM, Lonza) supplemented with 3% fetal bovine serum (FBS, BioSera), 1µM forskolin (Abcam), 4mM L-Glutamine (ThermoFisher), Glial Growth Factor (GGF, produced in lab), 100 µg/ml kanamycin (ThermoFisher), and 800 µg/ml gentamicin (ThermoFisher) and maintained at 10% CO₂ at 37°C. NSARafTR SCs were generated as described previously,⁵⁷ and cultured in the same medium. The J774A.1 mouse macrophage cell line was cultured in DMEM (Lonza) containing 10% FBS (BioSera), 200mM L-Glutamine (ThermoFisher), 100 µg/ml kanamycin (ThermoFisher) and 800 µg/ml gentamycin (ThermoFisher) at 10% CO₂ at 37°C. Human SCs were acquired from ScienCell and cultured in Schwann cell Medium (SCM, ScienCell) containing 5% FBS, Schwann cell Growth Supplement (SCGS) and Penicillin/streptomycin (P/S) to make complete SCM (ScienCell) at 37°C and 5% CO₂. The human macrophage THP1 cell line was kindly provided by Mark Marsh and cells were cultured in RPMI medium (Gibco) containing 10% FBS (BioSera) at 37°C and 5% CO₂.

Ex-vivo bridge cell isolation and culture

On Day 2 following injury, rat nerve bridges were collected, digested and ex vivo bridge cells isolated as described previously.¹⁴ To generate conditioned medium (CM), ex vivo bridge cells were washed twice in control medium (DMEM, low glucose, 1 g/l (Gibco) containing SATO mix (BSA 100 µg/ml, progesterone 60 ng/ml, putrescine 16 µg/ml, selenium 60 ng/ml, thyroxine 50 ng/ml, Tri-iodothyronine 50 ng/ml, transferrin 100 µg/ml, insulin 100 ng/ml) and incubated in control medium at hypoxic conditions (1.5% O₂) for a further 24 h. The CM was then collected and filtered (0.45µm pore size, Sarstedt) to be used in Boyden Chamber experiments.

To isolate macrophages and fibroblasts from Day 2 nerve bridges, panning plates were prepared by incubating bacterial plates with rabbit anti-mouse IgG (1/125, DAKO) in 50mM Tris pH 9.5 overnight at 4°C. The following day, plates were washed with PBS followed by incubation with antibodies against macrophages (1/1000, mouse CD11b/c Mas 370p clone Ox42, BD Biosciences), or fibroblasts (1/500, Thy1 clone Ox7) in MEM (Gibco) with 0.3% Bovine Serum Albumin (BSA, Sigma-Aldrich) for 1 h at room temperature (RT). Cells were then collected from Day 2 rat nerve bridges as previously described,¹⁴ and the cell suspension sequentially incubated on dishes coated with macrophage antibody for 10 min at RT, followed by three dishes coated with fibroblast antibody for 10 min at RT. Following antibody incubation, the dishes were washed with PBS and macrophages scraped and collected, while fibroblasts were trypsinised and collected. Both cell types were then plated at a density of 6x10⁴ cells/well in 24-well plates and incubated overnight at 37°C, 20% O₂ and 5% CO₂. The following day the cells were then washed twice in control medium and incubated at 1.5% O₂ for 24 h and either used for Boyden chamber assays, immunostaining, or harvested for RNA analysis.

NSΔRafER SCs differentiation assays

For the differentiation assays, NSΔRafTR SCs were washed and cultured in control medium containing SATO mix. Cells were then induced to differentiate by adding 1mM dbcAMP (Sigma-Aldrich), in the absence or presence of 100nM 4-hydroxytamoxifen (Sigma-Aldrich) in ethanol for 24 h.⁵⁷

Macrophage cell line hypoxia assays

To assess the J774A.1 cell line sensitivity to hypoxia, 1×10^4 cells were seeded onto PLL (Sigma-Aldrich) and laminin (Sigma-Aldrich) coverslips and 100 μ M pimonidazole HCl (hypoxyprobe-1 kit) was added before incubating the cells at normoxic (20% O₂), or hypoxic conditions (1.5% or 0.1% O₂) for 5 h. Cells were then washed for 15 min with RPMI with 10% serum (FBS), before immunostaining.

For RT-qPCR analysis, J774A.1 cells were seeded at a density of 1×10^5 per well in a 6-well dish (ThermoFisher) and THP1 cells at a density of 1×10^6 in a 75 cm² flask. To generate CM, 1×10^7 J774A.1 cells were seeded on a 15cm tissue culture plate. All cells were then incubated overnight in normoxic conditions (37°C, 20% O₂ and 5% CO₂). The following day cells were washed twice in control medium and incubated for 24 or 48 h at normal (20% O₂) or hypoxic conditions (1.5% O₂). Cells were either lysed in Trizol reagent (ThermoFisher) for RT-qPCR analysis, or the CM was collected and filtered (0.45 μ m pore size, Sarstedt) and used to either probe the Mouse Cytokine Array Panel A (ARY006, R&D Systems) following the manufacturer's protocol, protein analysis, or in migration assays.

Boyden chamber migration assay

For Boyden chamber migration assays, hanging cell culture inserts (Millipore, 5 μ m pore size for human SCs and 8 μ m for SCs) were coated with fibronectin (10 μ g/ml in MEM, Sigma-Aldrich) overnight. The next day SCs were harvested, washed twice in Control medium (DMEM, low glucose, 1 g/l containing SATO mix) and seeded at a density of 7.5×10^4 or 5×10^4 respectively into the upper compartment of Boyden chambers in duplicate before transferring into a 24-well plate. Control medium was used as a negative control, with serum (DMEM with 3% FBS) or 5 ng/ml VEGF-A¹⁶⁵ in Control medium (DMEM, Lonza) used as positive controls. Bridge fibroblasts, bridge macrophages, bridge CM, mouse macrophage cell line CM (from cells cultured at 20% O₂, 1.5% O₂ alone or treated with scrambled short interfering RNA (Scr siRNA) or CCL3 siRNAs 1–3), recombinant rat CCL3 at 10 and 50 ng/ml (R&D systems) and recombinant human CCL3 at 50 ng/ml (R&D systems) were used to test the role of macrophage derived CCL3 in SC migration. After 4 h incubation at 37°C and 10% CO₂, cells on the upper surface were removed mechanically and cells that had migrated onto the lower surface were fixed in 4% paraformaldehyde (PFA) and the nuclei counterstained with Hoechst. Images were quantified on the Axio Imager.A1 upright (Zeiss) at 20x, with positive nuclei from 8 different fields per condition quantified and expressed as fold migration change relative to control medium.

Dunn chamber migration assay

For Dunn chamber assays,⁵⁸ 2×10^4 SCs were seeded onto laminin (20 μ g/ml/MEM) and PLL coated glass coverslips and incubated overnight. The next day, cells were washed twice with Control medium (DMEM, low glucose, 1 g/l (Gibco) containing SATO mix). The coverslip was then inverted and placed onto the Dunn chamber, leaving an opening to remove the control medium from the outer reservoir using Whatmann paper. Control medium or medium either containing serum (3% FBS) or CCL3 (R&D systems), or mouse macrophage cell line CM (from cells cultured at 20% O₂, 1.5% O₂ alone or treated with Scr siRNA or CCL3 siRNAs 1–3) was then added to the outer reservoir and the coverslip was realigned centrally to ensure both reservoirs were covered. The chamber was then imaged using time-lapse microscopy at 10x using a Zeiss Axiovert 200M microscope at 37°C with 10% CO₂. Images were taken every 10 min for 24 h. Cells were then tracked by their nucleus using Velocity software (Improvision), with velocity measured and cell migration tracks created using macro plugins in Excel as described in.⁵⁹

Proliferation assay

2.5×10^4 SCs were seeded onto fibronectin and PLL coated glass coverslips and incubated overnight. Next day, the medium was changed in the morning and cells were washed with Control medium (DMEM low glucose plus SATO – insulin) (x4) in the afternoon and incubated in Control medium overnight. Cells were then stimulated with either serum, IGF-1 (100 ng/ml, Source BioScience), Neuregulin 1 (100 ng/ml, R&D Systems) or recombinant rat CCL3 (50 ng/ml, R&D systems), alone or in combination in normoxia. After 18 h, 5-ethynyl-2'-deoxyuridine (EdU, ThermoFisher) was added to the culture medium and cells were fixed 12 h later in 4% paraformaldehyde/PBS. Cells were then stained using the Click-iT EdU cell proliferation assay kit according to the manufacturer's instructions (ThermoFisher) and the nuclei were counterstained with Hoechst. To quantify cell proliferation, at least 200 nuclei from a minimum of 8 fields, from a minimum of 2 replicate coverslips, were counted on the Axio Imager.A1 upright (Zeiss) at 20x

Short interfering RNA knockdown

For siRNA transfection, siRNA knockdown was performed in J774A.1 cells and SCs using HiPerFect (Qiagen) using 5nM siRNA. siRNA target sequences:

CCL3 siRNA 1: 5'-CTAGGTAGACATGATGACAAA-3'

CCL3 siRNA 2: 5'-TTGTGACTATTATTCTGAA-3'

CCL3 siRNA 3: 5'-TCGAGGGACTCTCACTTGAA-3'

CCR1 siRNA: 5'-CAGACCCCTAGGTGTCACCAA-3'

Scr: 5'-AATTCTCCGAACGTGTCACGT-3'

Following knockdown with siRNA, cells were lysed in Trizol (ThermoFisher) and RNA isolated according to the manufacturer's instructions (ThermoFisher). RT-qPCR for CCL3 in J774A.1 cells and CCR1 in SCs was performed to validate the efficiency of the oligos at 48 h after knockdown.

RNA extraction and RTqPCR

Rat nerve stumps or bridges were collected Day 2 following injury and snap frozen in liquid nitrogen. Samples were crushed and homogenised on dry ice and then lysed in Trizol Reagent (ThermoFisher). Cultured cells were directly lysed in Trizol reagent (ThermoFisher) and RNA extracted according to the manufacturer's instructions (Invitrogen). After RNA purification including a DNase step, RNA was reverse-transcribed using either Super-Script II or IV Reverse Transcriptase (ThermoFisher). Quantitative PCR was then performed using the MESA Blue qPCR Kit (Eurogentec). Relative expression values for each gene of interest were obtained by normalising to B2M.¹²

Primers sequences

Rat CCL3

Fwd: 5'- CCATATGGAGCTGACACCCC-3'

Rev: 5'- TCTGCCGGTTCTCTGGTC-3'

Mouse CCL3

Fwd: 5'- CCATATGGAGCTGACACCCC-3'

Rev: 5'- AAATGACACCTGGCTGGGAG-3'

Human CCL3

Fwd: 5'- ACATCCGTCACCTGCTCAG -3'

Rev: 5'- TTGTTGCCAACAGCCACAC-3'

Rat CCR1

Fwd: 5'- CAAAGGCCAGAAACAAAGCC-3'

Rev: 5'- AGCCCCGAAGGCTTACAT-3'

Human CCR1

Fwd: 5'- GGTCTGGTCCTTGCAAT-3'

Rev: 5'- AGGGAAAGCGTGAACAGGAAG-3'

Rat MBP

Fwd: 5'- CACAAGAACTACCCACTACGG-3'

Rev: 5'- GGGTGTACGAGGTGTCACAA-3'

RNA-seq data analysis

The RNAseq database was reanalysed from a previous study.²⁸ Using Subio X Omics software, we processed the FASTQ files deposited in Gene Expression Omnibus (GSE103039) and performed DESeq2 analysis to compare the gene expression of ccr1, ccr5, cdh1 and Sox2 in SCs from intact nerves and compared to SCs from the nerve bridge and distal stump at day 4 post-injury.

Protein extraction from cell supernatant

Supernatant (CM) from J774A.1 cells was collected as described above and 10% volume of trichloroacetic acid (Sigma-Aldrich) was added followed by incubation at 4°C overnight. Protein was pelleted the next day by spinning for 10 min at 13,000 rpm at 4°C, washed once with 100% acetone (VWR) and spun again for 2 min at 13,000 rpm at 4°C. The supernatant was removed before drying the pellet and resuspending in Laemmli buffer (Biorad) containing β-mercaptoethanol (Sigma-Aldrich).

Western blot analysis

Western blot analysis was performed using Biorad western blot electrophoresis systems. Protein samples were resolved using Sodium Dodecyl Sulfate - polyacrylamide gel electrophoresis (SDS-PAGE). Protein was transferred onto nitrocellulose membranes (Millipore-Immobilon), which were subsequently blocked for 1 h at RT using 5% milk-TBST. The membrane was then incubated with primary antibodies to CCL3 (1/2000, Abcam, Ab25128) and β-actin (1/5000, Abcam, Ab8227) overnight at 4°C. The following day, the membrane was washed three times with TBST, followed by incubation with the appropriate secondary antibody conjugated to Horseradish peroxidase (HRP). Subsequently, membranes were washed three times with TBST before detection of proteins of interest with Pierce-ECL western blot substrate (ThermoFisher) or Luminata Crescendo Western HRP substrate (EMD-Millipore) using Imagequant LAS 4000.

Immunofluorescence

Sciatic nerves were dissected and fixed overnight in 4% PFA/PBS at 4°C, then cryoprotected in 30% sucrose/PBS overnight at 4°C. The following day, samples were incubated in 50% OCT/30% sucrose/PBS for 2 h and finally embedded in OCT before being frozen

in liquid nitrogen. Transverse (10 μ m) or longitudinal cryosections (60 μ m) were cut using a cryostat (Leica). Thin sections were permeabilised in 0.3% Triton/PBS for 30 min, washed and then blocked in 10% goat serum (Sigma-Aldrich)/PBS for 1 h. Thick sections were permeabilised and blocked in 0.3% Triton/10% goat serum/PBS for 2 h. Primary antibodies were diluted in 10% goat serum/PBS at the appropriate concentration and incubated overnight at 4°C. After washing, the appropriate fluorescent secondary antibody (1/400, Alexa Fluor 488, 594 or 647 from ThermoFisher) were used with Hoechst or DAPI to counterstain the nuclei for 1–2 h depending on the thickness of the section. Samples were mounted in Fluoromount G (ThermoFisher).

For MBP staining, longitudinal cryosections (10 μ m) were cut using a cryostat (Leica), and permeabilised for 20 min in 100% Methanol at –20°C. Following this, sections were washed in PBS 1X and the subsequent immunofluorescence protocol steps described above were performed.

For *in situ* hybridisation chain reaction (HCR) 10 μ m sections were washed twice with Diethyl pyrocarbonate (DEPC) PBS 1X (ThermoFisher), and then permeabilised with DEPC-EtOH 70% for 3 h at 4°C. Hybridisation was then performed using probes for CCL3 and/or CCR2 in hybridisation buffer (Molecular instruments) overnight at 37°C. The next day, sections were washed with Probe wash buffer (Molecular instruments) 4 times at 37°C before washing with SSCT 1X buffer. After this, an amplification step with meta-stable fluorescent DNA HCR hairpins targeting the probes (conjugated to Alexa Fluor 594 or 647, ThermoFisher) was performed overnight at RT. Sections were then washed again with SSCT 1X, incubated with DAPI (Sigma-Aldrich) and mounted with Fluoromount (ThermoFisher). For co-immunostaining, a post fixation step with 4% PFA was performed, followed by blocking with 5% donkey serum (Sigma-Aldrich) and incubation with Iba1 antibody (Wako) overnight at 4°C. Finally, sections were washed again with DEPC-PBS 1X and incubated with secondary antibody Alexa Fluor 594 (ThermoFisher) and DAPI (Sigma-Aldrich) before mounting with Fluoromount.

For staining of macrophages or fibroblasts isolated from the nerve bridge, cells were grown on glass coverslips and fixed using 4% PFA for 10 min. Cells were then permeabilised with 0.3% Triton in PBS for 10 min and coverslips were blocked using 3% bovine serum albumin (BSA, Sigma-Aldrich) and either immunolabelled with primary antibodies to macrophages (Iba1, Wako) or fibroblasts (Prolyl4hydroxylase beta, Origene) overnight at 4°C. Coverslips were then washed with PBS and incubated with secondary antibodies conjugated to AlexaFluor for 1 h, and then mounted onto microscope slides using Fluoromount G (ThermoFisher).

For staining of J774A.1 cells, the hypoxyprobe-1 kit was used according to the manufacturer's instructions.

Immunofluorescence antibodies

The following primary antibodies were used for immunofluorescence staining at the indicated dilutions: CD31 (1/50, BD Pharmingen 553370), CD31 (1/1000, R&D AF3628), S100 (1/100, Dako Z0311), Iba1 (1/400, Wako 019–19741), mouse-F4/80 (1/500 AbD Serotec MCA497), MBP (1:1000, ThermoFisher PA1-10008), neurofilament 200kD (NF, 1/1000, Abcam ab4680), β -tubulin III (1/1000, Biolegend 802001), Prolyl4hydroxylase beta (1/1000 Origene AF5110-1), p75NTR (1:300, EMD Millipore 07–476). Alexa-Fluor secondary antibodies were obtained from Invitrogen, and Horseradish peroxidase (HRP)-linked antibodies were purchased from GE-healthcare.

Image analysis

All confocal images were acquired using either an inverted SPE confocal microscopes (Leica) or a LSM900 microscope (Zeiss). For each experiment, images were acquired using the same microscope settings. All images were then opened in Fiji software, and the same volume and number of z-stacks were taken for analysis.

To quantify macrophage and fibroblast numbers after panning and immunofluorescence, for each experiment, positive Iba1 (macrophages) or Prolyl4hydroxylase beta (fibroblasts) nuclei were quantified from 20 different images from duplicate coverslips and expressed as a percentage of positive cells. To analyze the effect of hypoxia on J774A.1 macrophages after immunofluorescence, 300 to 500 nuclei per condition from each experiment were counted as positive or negative for hypoxyprobe-1 and expressed as a percentage of positive cells.

To analyze longitudinal sections of injured nerves, images were acquired from the proximal to distal stump, in order to incorporate the entire bridge region. For CCL3 injection experiments, image projections were merged using Adobe Photoshop software, resulting in tile-scan images. For all other nerve injury experiments, tile-scan images were automatically stitched by Leica software after acquisition.

To quantify the effects of CCL3 injection and inhibition on blood vessels, SCs and axons, the area corresponding to the nerve bridge was selected, thresholded and made binary using Fiji software. The Create Selection function was used to automatically outline the thresholded area and the immunostained area quantified using the measurement function. The area of positive staining was expressed as fold change compared to control animals.

To quantify macrophage density, five higher magnification images corresponding to the nerve bridge or three images from uncut nerves were selected per animal, and nuclei that were positive for F4/80 staining counted. For SC/blood vessel association at Day 90, two higher magnification images per animal of aberrant regions of CCL3 KO mice were selected and the number of SCs in contact with BV quantified. An SC was considered in contact with a blood vessel if eGFP and CD31 colocalised. To quantify MBP and p75 colocalization in SCs at Day 90, three higher magnification images per animal of aberrant and regenerated regions of CCL3 KO mice were selected and the number of SCs colocalising with MBP and p75 were quantified.

To quantify SC cord and axonal deviation from the vertical of the proximal to distal axis, the SC cords or axons were traced in Fiji and the angle of each SC cord or axon measured. The angle of deviation was calculated relative to the proximal/distal nerve axis and

expressed as deviation from the vertical. For HCR experiments, three images per animal were acquired from the proximal, bridge and distal regions of injured sciatic nerves. For each image, a z-projection was made using Fiji software and an equal Gaussian Blur filter was applied for channels with mRNA puncta for smoothing. The number of CCL3 puncta per nuclei was counted in each region and expressed as the fold change from the proximal stump. In order to assess which cell type predominately expressed CCL3, the number of CCL3 puncta per nuclei was quantified in samples co-stained with Iba1 or probes for CCR2.

Electron microscopy

Sciatic nerves were collected and fixed in 0.12M phosphate buffered solution containing 2% glutaraldehyde before incubation in 2% Osmium Tetroxide overnight at 4°C. The samples were further stained in 2% uranyl acetate for 45 min at 4°C and washed in water before dehydration by incubation in a series of increasing concentrations of ethanol. Nerves were then transferred to propylene oxide, before gradual infiltration in Epon resin via 1:1 propylene oxide:Epon mix, followed by 100% Epon overnight, fresh 100% Epon for several hours the following day and finally polymerisation at 60°C overnight. Samples were trimmed and 70nm ultrathin sections were cut with a 45° diamond knife (DiatomeDiATOME) using an ultramicrotome (Leica UC7) and collected on 1 × 2mm Formvar-coated slot grids. Images were acquired with a FEI Tecnai Spirit Bio-twin electron microscope (ThermoFisher) and a Morada camera (Olympus Soft Imaging Solutions). Using Fiji software, the number of myelinating SCs were quantified from 5 images per sample.

QUANTIFICATION AND STATISTICAL ANALYSIS

All statistical analysis were performed using GraphPad Prism software (v10). Comparisons between two groups was performed using an unpaired, two-tailed Student's t-test except when calculating angle deviations, where unpaired, two-tailed Welch's correction t test was applied. A one-way analysis of variance (ANOVA) with Tukey's multiple comparisons test was used to compare more than two groups. Statistical differences were considered to be significant when $p < 0.05$, as indicated in the Figures. Statistical details for each experiment as well as n values are provided in each of the figure legends. All data are expressed as mean value ± SEM. P-values are indicated by asterisks as follows: * $p < 0.05$, ** $p < 0.01$, *** $p < 0.001$, **** $p < 0.0001$.